Applied Mathematical Modelling 37 (2013) 9242–9268

Contents lists available at SciVerse ScienceDirect

Applied Mathematical Modelling

journal homepage: www.elsevier.com/locate/apm

An improved isogeometrical analysis approach to functionally graded plane elasticity problems

B. Hassani [a,*], A.H. Taheri [a], N.Z. Moghaddam [b]

[a] Mechanical Engineering Department, Ferdowsi University of Mashhad, P.O. Box 91775-1111, Mashhad, Iran
[b] Department of Civil Engineering, Shahrood University of Technology, Shahrood 36155, Iran

ARTICLE INFO

Article history:
Received 7 June 2012
Received in revised form 2 March 2013
Accepted 8 April 2013
Available online 10 May 2013

Keywords:
Generalized isogeometrical analysis
Functionally graded materials
Non-Uniform Rational B-Splines (NURBS)

ABSTRACT

The isogeometric analysis method is extended for addressing the plane elasticity problems with functionally graded materials. The proposed method which employs an improved form of the isogeometric analysis approach allows gradation of material properties through the patches and is given the name Generalized Iso-Geometrical Analysis (GIGA). The gradations of materials, which are considered as imaginary surfaces over the computational domain, are defined in a fully isoparametric formulation by using the same NURBS basis functions employed for the construction of the geometry and the approximation of the solution. The basic concept of the developed approach is concisely explained and its relation to the standard isogeometric analysis method is pointed out. It is shown that the difficulties encountered in the finite element analysis of the functionally graded materials are alleviated to a large degree by employing the mentioned method. Different numerical examples are presented and compared with available analytical solutions as well as the conventional and graded finite element methods to demonstrate the performance and accuracy of the proposed approach. The presented procedure can also be employed for solving other partial differential equations with non-constant coefficients.

1. Introduction

Several numerical methods have been proposed for the solution of partial differential equations. The Non-Uniform Rational B-Splines (NURBS) based isogeometric analysis (IGA) introduced by Hughes et al. [1] in 2005 as an innovative numerical methodology for the analysis of PDE problems, letting for the exact modeling of CAD type geometries. Up to now, this method has been applied to various types of field problems including structural analysis e.g. [2–5], fluid–structure interaction [6–8], heat transfer [9], etc. It is noted that all the published papers are dealing with the analysis of different types of structures with homogeneous materials. But this paper presents a slightly different and more general perspective of the IGA method, with the ability of analysis of structures with nonhomogeneous materials. In order to demonstrate this ability, it is applied to the analysis of functionally graded plane elasticity problems which are explained below briefly.

1.1. Functionally graded materials

Functionally graded materials (FGM) are kind of heterogeneous materials that often possess better mechanical, thermal or electrical performances in comparison with the traditional homogeneous objects [10]. These materials are a new gener-

* Corresponding author.
E-mail address: b_hassani@um.ac.ir (B. Hassani).

0307-904X/$ - see front matter © 2013 Elsevier Inc. All rights reserved.
http://dx.doi.org/10.1016/j.apm.2013.04.048

ation of advanced inhomogeneous composite materials that were originally proposed for thermal barriers of modern engineering structures in extremely high temperature environments and have been increasingly applied since then [11]. They are now being regarded as one of the most promising candidates for future smart composites in many engineering disciplines [12]. FGMs may exhibit isotropic or anisotropic properties depending on the processing technique and the practical engineering requirements. The material properties of FGMs demonstrate a continuous and smooth change from one side of an object to the other by gradually varying the volume fraction of constituent materials that leads to elimination of the interface and layering problems. By functional gradation, new properties can be obtained that can improve both material and component structures to achieve higher performance and material efficiency [13]. A considerable part of studies on FGMs is devoted to thermal stress and fracture analysis in structures such as plates and shells, e.g. see [14–19].

Besides the problem of proper manufacturing of the material, design of the parameters and analysis of such heterogeneous materials is a challenge for the engineering community [20]. Due to the high cost and difficulties of experimental tests for material design, the mathematical theory of homogenization [21–24] may be employed for determination of the microscopic properties of the composite constituents that is the subject of our further research.

1.2. Techniques of analysis of FGM problems

Assuming that we are able to manufacture FGMs, still some difficulties may arise when the conventional computational methods, such as finite elements, are employed for their stress analysis. To circumvent some of these problems, in this research work, the applicability of the NURBS based analysis is investigated.

A key feature that distinguishes FGMs from homogeneous materials is that the mechanical, electrical and thermal properties of the material vary spatially. Thus, the analysis of functionally graded materials is significantly more complex than the homogeneous case. By now, for the analysis, either analytical techniques or numerical methods such as finite elements have already been employed for certain problems.

Due to the complexity of the analysis, depending on the materials anisotropy and inhomogeneity, only limited cases are solved by analytical methods. Most of the closed form solutions for non-homogeneous materials are carried out under the simplifying assumption of material isotropy.

The most common numerical approach adopted for the analysis of FGM problems is the FE method in which the domain of the problem is usually divided into different regions with constant mechanical properties. In other words, multiple dissimilar materials are assigned to different elements which results in discontinuity of the solution on elements borders. Besides, it involves some extra approximation and to obtain acceptable results fine meshes are required that considerably increase the computational effort [13,25,26].

Moreover, two other different methods have been proposed for modeling the gradation of material properties in the FEM thus far, which employ the so-called graded elements. The formulations of these methods differ in the method of sampling the materials variations through each element. In 2000, Santare and Lambros [27] presented a graded finite element approach for modeling the behavior of nonhomogeneous materials. The procedure was applied to a typical two-dimensional plane stress element with linear interpolation shape functions. However, the results are applicable to other types of elements. In this approach, that is given the name ‘‘graded finite element’’ by the authors, the material properties are sampled directly at the gauss points by employing the available explicit functions assumed for the gradation of the materials.

Two years later, Kim and Paulino [13] proposed a generalized isoparametric formulation of the FEM which extended the FEM to variable elasticity materials. In this approach, an alternative numerical finite element model named ‘‘generalized isoparametric graded finite element’’ is proposed, where the authors adopt the same shape functions to interpolate the unknown displacements, the geometry and the mechanical parameters, in a generalized fully isoparametric formulation [13]. In this approach the material properties are mapped onto the nodes of the finite elements description and interpolated at the Gauss points by the same shape functions that are used for approximation of displacements [28].

Although these methods are different, they yield similar results for fine mesh discretizations [13]. It is believed that the generalized isoparametric formulation is more natural to the finite element method than the Gauss point sampling of material properties. Regarding the fact that the generalized formulation embraces the important isoparametric concept, the same shape functions are used to interpolate the unknown displacements, the geometry and the material properties [13]. This formulation which can be considered as the extension of FEM to variable elasticity materials can be applied to isotropic or anisotropic FGMs assuming the homogenization approach [28]. This concept is also employed in some other types of numerical methods. Typically, an analogous procedure is employed in a high-order control volume finite element method [29] for thermo-elastic analysis of functionally graded plane elasticity problems.

This article investigates the applicability of both the mentioned concepts in isogeometric analysis of FGMs by allowing for gradation of material properties through the patches, but concentrates on the isoparametric formulation. It will be seen that implementation of the isoparametric formulation in isogeometric analysis of FGMs is not as easy as in FEM and needs an extra step of interpolation.

Furthermore, the boundary element method (BEM) is applied to FGMs as well, provided that the Fundamental Solution (FS) of the material is known either analytically or numerically [28]. The application of BEM to variable elasticity is well known since 1993 by work of Sladek et al. [30] where the boundary element method for nonhomogeneous elasticity is described. A field boundary element method (FBEM) was presented and compared with generalized isoparametric FEM by Minutolo et al. [28] in 2009. The comparison showed that both methods give results with similar good accuracy. The application

of meshfree methods to dynamic analysis of sandwich beans with FGM core and vibration analysis of laminated composite plates were also investigated by Bui et al. [31,32]. Finally, in recent years some other numerical methods have been introduced for the analysis of FGMs. For instance, in 2011 Chareonsuk and Vessakosol presented the numerical solutions for functionally graded solids under thermal and mechanical loads using a high-order control volume finite element method [29]. In one of the latest numerical works, the FBEM is extended for the analysis of multiregion functionally graded materials [33]. In addition, free vibration and buckling analysis of laminated composite plates is investigated by Shojaee et al. [34] by using the NURBS based isogeometric analysis method. Finally, recently Valizadeh et al. [35] used the IGA method to study the static and dynamic characteristics of FGM plates. The material properties are assumed to be graded only through the plate thickness and static bending, mechanical and thermal buckling, linear free flexural vibration and supersonic flutter analysis of FGM plates are numerically studied. Refs. [25,36–39] can be consulted for a thorough review of the literature on the subject.

1.3. Isogeometric analysis method

The isogeometric analysis method, which can be considered as a logical extension of the finite element method, is more geometrically based and takes inspiration from Computer Aided Design (CAD). It is a generalization of the classical finite element analysis and has many features in common with it. The gist of the IGA method is combining the CAD and FEM for removing the need for a conventional mesh by using *knot elements* instead of *finite elements*. A 'knot element' is part of a curve, (surface and volume in two and three dimensional problems, respectively), that is formed by a specific knot span, (or by their tensor products in higher dimensions), when B-Splines are employed. The primary advantage of this method is being geometrically precise, no matter how coarse the discretization is. It simplifies mesh refinement by eliminating the needs for communication with the CAD models and results in a considerable reduction in the size of system of equations which is cost effective and makes it a potential and promising substitute to the other numerical methods [1,2,40–42].

It is noted that the implementation of the conventional adopted concept in the FEM for the analysis of FGMs, i.e. capturing the variations of material properties by using a large number of homogeneous elements is not applicable to IGA. Because, in this case, patches play the role of elements in the FEM, i.e. the material properties are supposed to be constant throughout each of the patches; then it is required to use a large number of patches for this purpose which is not practical. Therefore, the only practical way for the analysis of problems with graded materials seems allowing variations of the material properties within the IGA patches that are usually much larger subdomains in comparison to the finite elements. In analogy to the finite element 'graded elements' we might use the terminology 'graded patches' to identify them in this research.

1.4. Inspiration of GIGA

The suggested approach is based on the idea that in the isogeometric analysis method, we can consider the variations of the solution of differential equations (field variables in most of engineering problems) as imaginary surface(s) over the computational domain that are constructed by using advanced versions of Splines such as NURBS. So, in the same manner, the coefficient terms of differential equations, which themselves might be functions in general, can be assumed as other imaginary surfaces over the domain which can also be stated by using the same NURBS basis functions. The inspiration of the presented perspective came from the impressive progresses in computer aided geometry design (CAGD) technologies, and using their abilities in creating complex surfaces, for solving partial differential equations (PDE) which could not be easily handled by other numerical methods [43]. The surfaces of the coefficients can be constructed by using NURBS so that their defining parameters (i.e. the appropriate imaginary heights of the control points) are obtained by employing NURBS interpolation techniques, while the defining parameters of the solution surface(s) are considered as unknowns that have to be evaluated by criteria which can be extracted from the governing equation (e.g. minimization of the total potential energy) [43,44]. This issue is clearly visualized in Fig. 3(a)–(c) of section 3-2 for the better insight. As pointed above, this approach, in fact, can be considered as the generalization of the standard IGA method to variable elasticity. It will be seen that employing the mentioned perspective will lead to a fully isoparametric formulation for the analysis of variable elasticity problems.

Due to the possibility of simultaneously modeling of the structural shape and the material distribution, GIGA constitutes an important tool for studying integrated modeling and analysis of FGMs. In addition, this method, besides being independent of a mesh generation tool, has some extra advantages over the conventional FEM such as ending up with smaller system of equations and consuming less computational time. Since in this approach graded patches are employed, in which variations of materials are captured by using NURBS interpolation, the material gradations can be modeled with a high accuracy even by employing a single patch and quite a few numbers of control points. We also believe that the proposed perspective facilitates the imagination and interpretation of the problem definition and solution.

One of the other most prominent applications of the proposed method is in material design and optimization problems, which is the subject of our further research [45]. Whereas in this approach variations of material properties are modeled by using NURBS, it provides a high powered tool for creating any complex material distribution profile employing quite a few numbers of control points. In addition, any desired level of material distribution continuity is available which results in creating very smooth material profiles that are easy to fabricate. Furthermore, because the distribution of material properties are captured in a fully isoparametric formulation by using the same net of control points and basis functions employed for the construction of the geometry, computational effort is considerably decreased. It also provides some extra advantages in this category which are discussed in details in [45].

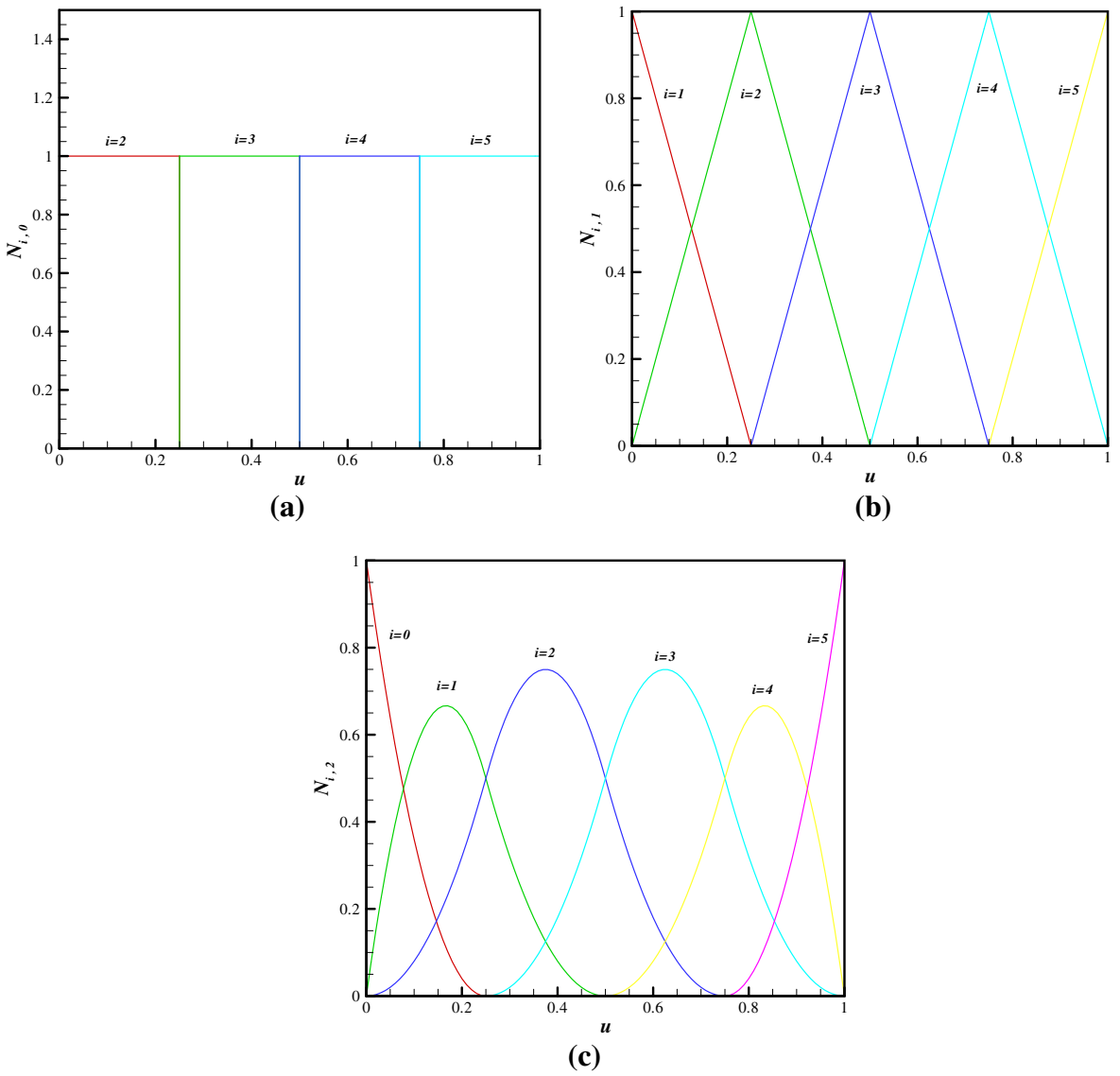

Fig. 1. Basis functions of (a) order 0, (b) order 1 and (c) order 2.

1.5. Article structure

In the following sections, a unified approach is presented which employs an isogeometrical method for both modeling and analysis of the FGM plane problems. The constitutive material matrix is considered to be either isotropic or orthotropic at each point where the elastic modulus is assumed to vary continuously throughout the domain according to an assumed law of distribution. Since in GIGA the variations of the displacement coordinates as well as the mechanical properties of the problems are considered as imaginary surfaces, Section 2 is devoted to the preliminary introduction to the surface generation. The derivation of the numerical formulation of plane elasticity problems with FGMs by employing the GIGA method is discussed in Section 3. Some numerical examples are solved in Section 4 to demonstrate the efficiency of the proposed method. Finally, conclusions and suggested further research is the subject of Section 5.

2. Surface definition by Splines

Since, as mentioned above, the main idea behind the IGA method is that any component of the sought answer is imagined as a surface which can be generated by using Splines and NURBS, a brief description of the technique is here introduced. Some of the concepts and parameters of the approach are concisely explained in the following.

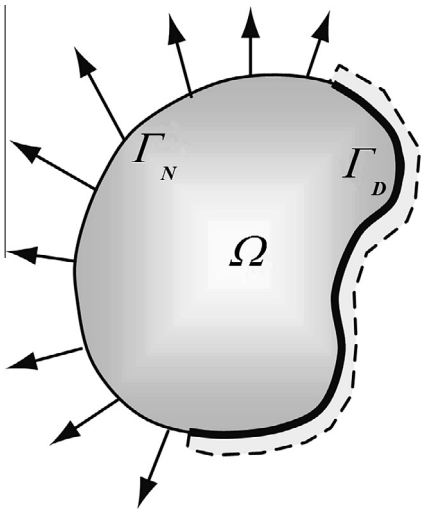

Fig. 2. Definition of the domain in a boundary value problem.

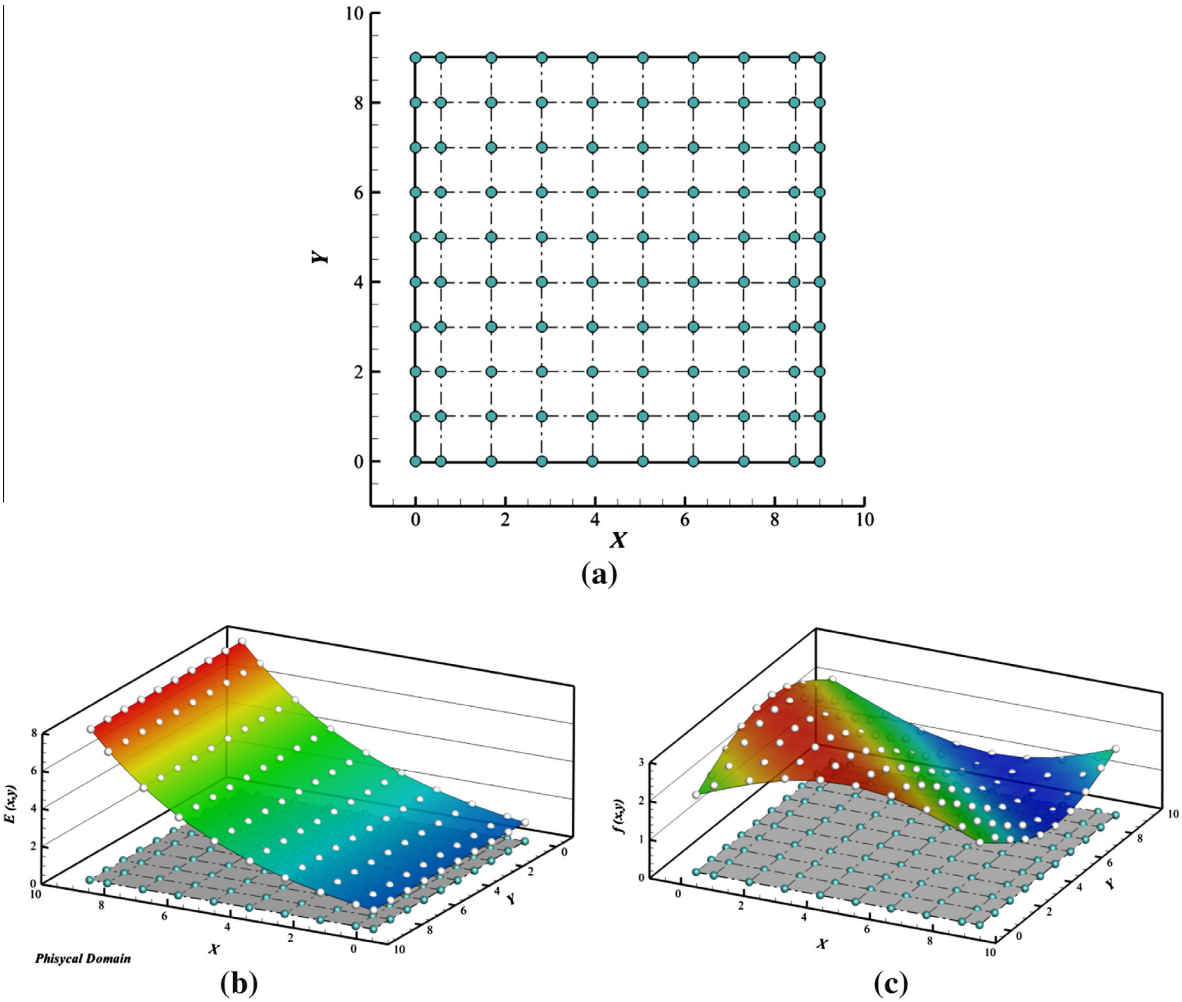

Fig. 3. (a) A typical square domain with the net of control points (b) variations of Young's modulus (c) variations of a typical field variable.

2.1. The knot vector

A knot vector **U** is a set of non-decreasing real numbers representing coordinates in the parametric space of the curve:

$$\mathbf{U} = \{u_0, u_1, \ldots, u_m\}, \tag{1}$$

where m is the number of knots and equals to $n + p + 1$. Also, n is the number of basis functions that is related to the number of control points and p is the degree of the B-Spline basis functions (order $p + 1$). A knot vector is said to be uniform if its knots are uniformly spaced, otherwise it is non-uniform. Moreover, a knot vector is said to be open if its first and last knots are repeated $p + 1$ times like (2).

$$\mathbf{U} = \left\{ \underbrace{0, \ldots, 0}_{p+1}, u_{p+1}, \ldots, u_{m-p-1}, \underbrace{1, \ldots, 1}_{p+1} \right\}. \tag{2}$$

The interval $[u_0, u_m]$ is called a patch, whereas the interval $[u_i, u_{i+1}]$ is called a knot span. In the following, we always utilize open knot vectors for solving the problems as their knots start by 0 and ends by 1.

2.2. B-Spline basis functions

Basis functions formed from open knot vectors are interpolators at the ends of the parametric interval $[r_0, r_{n+p+1}]$, but are not in general interpolator at interior knots. The ith B-Spline basis function of degree p, denoted by $N_{i,p}(u)$, is defined recursively as:

$$\begin{aligned} N_{i,0}(u) &= \begin{cases} 1 & \text{if} \quad u_i \leqslant u \leqslant u_{i+1} \\ 0 & \text{otherwise}, \end{cases} \\ N_{i,p}(u) &= \frac{u - u_i}{u_{i+p} - u_i} N_{i,p-1}(u) + \frac{u_{i+p+1} - u}{u_{i+p+1} - u_{i+1}} N_{i+1,p-1}(u). \end{aligned} \tag{3}$$

For example, for $p = 0, 1, 2$ and using a uniform knot vector $\mathbf{U} = \{0, 0, 0, 0.25, 0.50, 0.75, 1, 1, 1\}$ some of the basis functions are shown in Fig. 1(a)–(c). For more details Refs. [46–48] can be consulted.

2.3. Creating surfaces by using NURBS

A NURBS surface is parametrically constructed as

$$\mathbf{S}(r, s) = \frac{\sum_{i=0}^{n_1} \sum_{j=0}^{n_2} N_{i,p}(r) N_{j,q}(s) w_{ij} \mathbf{P}_{ij}}{\sum_{k=0}^{n_1} \sum_{l=0}^{n_2} N_{k,p}(r) N_{l,q}(s) w_{kl}} \quad \begin{matrix} 0 \leqslant r \leqslant 1 \\ 0 \leqslant s \leqslant 1, \end{matrix} \tag{4}$$

where **U** and **V** are the knot vectors

$$\begin{aligned} \mathbf{U} &= \left\{ \underbrace{0, \ldots, 0}_{p+1}, r_{p+1}, \ldots, r_{m_1-p-1}, \underbrace{1, \ldots, 1}_{p+1} \right\} \\ \mathbf{V} &= \left\{ \underbrace{0, \ldots, 0}_{q+1}, s_{q+1}, \ldots, s_{m_2-q-1}, \underbrace{1, \ldots, 1}_{q+1} \right\}, \end{aligned} \tag{5}$$

and

$$\mathcal{R}_{ij}^{p,q}(r, s) = \frac{N_{i,p}(r) N_{j,q}(s) w_{ij}}{\sum_{k=0}^{n_1} \sum_{l=0}^{n_2} N_{k,p}(r) N_{l,q}(s) w_{kl}}. \tag{6}$$

Also, $\mathbf{P}_{ij}$ are $(n_1 + 1)(n_2 + 1)$ control points, w_{ij} are the associated weights to every control points and $N_{i,p}(r)$ and $N_{j,q}(s)$ are the normalized B-Splines basis functions of degree p and q. In brief, we can write the NURBS surface as:

$$\mathbf{S}(r, s) = \sum_{i=0}^{n} \sum_{j=0}^{m} \mathcal{R}_{ij}^{p,q}(r, s) \mathbf{P}_{ij}, \tag{7}$$

where $m_1 = n_1 + p + 1$ and $m_2 = n_2 + q + 1$

2.4. Curve and surface interpolation by NURBS

In order to solve the differential equations via the GIGA method, the coefficient functions of differential terms must be stated in terms of NURBS parameters, i.e. control points and knot vectors, using the NURBS interpolation algorithms. There

are many subtleties in fitting, and literally hundreds of papers have been written on this topic [47]. Many of the techniques are heuristic, and there are usually no unique or clear-cut "right" answers. The most common algorithms are global algorithms which select an appropriate knot vector and set up a system of linear equations that yields the control points coordinates. Various interpolation algorithms usually differ in the methods of parameterization, and also selecting the appropriate knot vectors for the constitution of system of equations. However, the existing algorithms are not of interest in this paper because it will be seen that they cannot be utilized in GIGA approach. The reason will be explained in details in the subsequent sections.

3. Derivation of numerical formulation

3.1. Elasticity formulations in brief

We recall the governing elliptic equations for a general static linear elasticity problem in a domain $\Omega \in \mathbb{R}^d$ with boundary Γ is

$$\sigma_{ij,j} + f_i = 0 \text{ in } \Omega, \quad 1 \leqslant i,j \leqslant d, \tag{8}$$

where d denotes the dimension of problem, f_i are the components of the body force and σ_{ij} represent second-order stress tensor. According to the general Hook's law

$$\sigma_{ij} = c_{ijkl}\varepsilon_{kl}, \quad 1 \leqslant i,j,k,l \leqslant d, \tag{9}$$

where c_{ijkl} are the fourth-order elasticity tensor and $c_{ijkl} = c_{jikl} = c_{ijlk} = c_{klij}$. Also, ε_{kl} are the linearized second-order small strain tensor which are defined as

$$\varepsilon_{kl} = \frac{1}{2}(u_{k,l} + u_{l,k}), \quad 1 \leqslant k,l \leqslant d, \tag{10}$$

where u_k represent the displacement vector. The Dirichlet boundary conditions are defined on $\Gamma_D \subset \Gamma = \partial\Omega$ which typically we assume that $u = 0$ on Γ_D and the Neumann conditions on Γ_N are defined by

$$\sigma_{ij}n_j = t_i, \tag{11}$$

where $\Gamma_N \cap \Gamma_D = \emptyset$ and n_j are the unit vectors of the coordinate system. See Fig. 2.

Now, we extract the relations needed for the two dimensional FGM plane elasticity problems $(i = 1,2)$ and hereafter we make use of x and y instead of 1 and 2, respectively. Eq. (7) can be written in a new form as

$$\mathbf{D}\boldsymbol{\sigma} + \mathbf{f} = \mathbf{0}, \tag{12}$$

where $\mathbf{D}$ denotes the differential operator and is defined by

$$\mathbf{D} = \begin{bmatrix} \partial/\partial x & 0 & \partial/\partial y \\ 0 & \partial/\partial y & \partial/\partial x \end{bmatrix}, \tag{13}$$

and $\mathbf{f}$ and $\boldsymbol{\sigma}$ denote the body force and stress vectors as shown in Eqs. (13) and (14), respectively.

$$\mathbf{f} = \{ f_x \quad f_y \}^T, \tag{14}$$

$$\boldsymbol{\sigma} = \{ \sigma_{xx} \quad \sigma_{yy} \quad \sigma_{xy} \}^T. \tag{15}$$

It should be noted that, in plane problems, we use C_{ij} instead of c_{ijkl} that can be expressed in terms of the engineering constants (E, ν, G) which are the elastic modulus, Poisson's ratio and shear modulus, respectively.

In the FGMs, the elements of the constitutive matrix can vary continuously through the domain. But in most of the literature, the elastic modulus is considered as a varying function where the other parameters are assumed constants. Typical analytical studies on the FGMs have assumed linear, exponential, and power-law variations in elastic modulus as in Eqs. (15)–(17), respectively:

$$C_{ij}(x) = C^o_{ij}(1 + ax), \tag{16}$$

$$C_{ij}(x) = C^o_{ij}\exp(ax), \tag{17}$$

$$C_{ij}(x) = C^o_{ij}x^a, \tag{18}$$

where x is the specified spatial coordinate and C^o_{ij} and a are set to constants. It is understandable that by substituting (15)–(17) into the governing differential equations, generally more complicated relations are generated. In this case, solution is naturally more difficult and hence limited cases of the analytical solutions of FGMs have been reported thus far.

As we know, plane elasticity problems are either plane stress (*PSS*) or plane strain (*PSN*), where the only difference is in their elasticity matrix. As it was pointed out previously, by assuming a constant Poisson's ratio, ν, and a continuous variation

in the elastic modulus throughout the domain, $E(x,y)$, the constitutive matrix for the *PSS* and *PSN* cases will be as Eqs. (18) and (19), respectively.

$$C_{PSS} = E(x,y)\begin{bmatrix} \frac{1}{1-\nu^2} & \frac{\nu}{1-\nu^2} & 0 \\ \frac{\nu}{1-\nu^2} & \frac{1}{1-\nu^2} & 0 \\ 0 & 0 & \frac{1}{2(1+\nu)} \end{bmatrix}, \tag{19}$$

and

$$C_{PSN} = E(x,y)\begin{bmatrix} \frac{1-\nu}{1-\nu-2\nu^2} & \frac{\nu}{1-\nu-2\nu^2} & 0 \\ \frac{\nu}{1-\nu-2\nu^2} & \frac{1-\nu}{1-\nu-2\nu^2} & 0 \\ 0 & 0 & \frac{1}{2(1+\nu)} \end{bmatrix}. \tag{20}$$

3.2. Generalized isogeometrical formulation

In the IGA solution of plane problems, further to the x and y coordinates of the control points which are employed for the geometrical modeling of the domain of problem, a couple of extra coordinates are considered as the unknown variables to be determined via the criteria which is obtained from the governing differential equation. Following a conventional variational approach, similar to the finite element method, the functional of total potential energy of Eq. (20) can be obtained and its stationary conditions with respect to the approximation parameters results in the system of equations to be solved.

$$\Pi = \frac{1}{2}\mathcal{B}(\mathbf{u},\mathbf{u}) - \ell(\mathbf{u}). \tag{21}$$

Here, $\mathbf{u} = \{u, v\}^T$ is the displacement vector and the bilinear and linear parts of the total potential energy functional in a Cartesian coordinate system are

$$\mathcal{B}(\mathbf{u},\mathbf{u}) = h_e \oint_{\Omega_e} \left[C_{11}\left(\frac{\partial u}{\partial x}\right)^2 + 2C_{12}\frac{\partial u}{\partial x}\frac{\partial v}{\partial y} + C_{22}\left(\frac{\partial v}{\partial y}\right)^2 + C_{66}\left(\left(\frac{\partial u}{\partial y}\right)^2 + 2\frac{\partial u}{\partial y}\frac{\partial v}{\partial x} + \left(\frac{\partial v}{\partial x}\right)^2\right)\right] dxdy, \tag{22}$$

and

$$\ell(\mathbf{u}) = h_e \oint_{\Omega_e} (uf_x + vf_y)dxdy + h_e \oint_{\Gamma_e} (ut_x + vt_y)d\Gamma, \tag{23}$$

respectively. Here, $\{f_x, f_y\}^T$ and $\{t_x, t_y\}^T$ are the vectors of the body forces and tractions, C_{11}, C_{12}, C_{22} and C_{66} are the elements of the constitutive matrix and h_e denotes the thicknesses of the used patches in the plane stress case, which is equal to unity for plane strain problems. Ω and Γ represent the domain of the patch and its boundary, respectively. Now, let the unknown displacement components u_x and u_y be approximated by B-Spline basis functions as

$$u_x(r,s) \approx \sum_{i=0}^{n_1}\sum_{j=0}^{n_2} \mathcal{R}_{ij}^{p,q}(r,s)U_{ij}^x, \tag{24}$$

$$u_y(r,s) \approx \sum_{i=0}^{n_1}\sum_{j=0}^{n_2} \mathcal{R}_{ij}^{p,q}(r,s)U_{ij}^y, \tag{25}$$

where r and s are the B-Spline basis function parameters, U_{ij}^x and U_{ij}^y are the altitudes of the control points and $\mathcal{R}_{ij}^{p,q}(r,s)$ is defined in Eq. (5). These relations can be summarized as

$$\mathbf{u} = \begin{Bmatrix} u_x \\ u_y \end{Bmatrix} = \mathbf{N}\mathbf{\Delta}. \tag{26}$$

It is noted that the net of control points that lies, topologically, on a rectangle in the r and s parametric space, can be defined by the integer i and j indices alongside the coordinates axes. However, in order to simplify the process of assembly of patches, a single parameter, α, is employed which is defined by a convertor function, $\mathcal{C}(i,j)$, as

$$\alpha = \mathcal{C}(i,j) = (i+1) + j(n+1), \begin{cases} 0 \leqslant i \leqslant n_1 \\ 0 \leqslant j \leqslant n_2, \end{cases} \tag{27}$$

and $\alpha = 0, 1, \ldots, (n_1+1)(n_2+1) - 1$. Hence, we can write $\mathcal{R}_{\alpha}^{p,q}$ and U_{α} in lieu of $\mathcal{R}_{ij}^{p,q}$ and U_{ij}, respectively. If we define the matrix $\mathcal{N}$ and the vector $\mathbf{\Delta}$ by Eqs. (27) and (28)

$$\mathcal{N} = \begin{bmatrix} \mathcal{R}_0^{p,q} & 0 & \mathcal{R}_1^{p,q} & 0 & \dots & \mathcal{R}^{p,q}_{(n_1+1)(n_2+1)-1} & 0 \\ 0 & \mathcal{R}_0^{p,q} & 0 & \mathcal{R}_1^{p,q} & \dots & 0 & \mathcal{R}^{p,q}_{(n_1+1)(n_2+1)-1} \end{bmatrix}, \tag{28}$$

and

$$\mathbf{\Delta} = \{ U_0^x \quad U_0^y \quad U_1^x U_1^y \quad \dots \quad U^x_{(n_1+1)(n_2+1)-1} \quad U^y_{(n_1+1)(n_2+1)-1} \}^T, \tag{29}$$

the strains and stresses can be defined by (29) and (30) which are the same as the conventional finite element procedure

$$\boldsymbol{\varepsilon} = \mathbf{D}^T\mathbf{u} = \mathbf{D}^T\mathbf{N}\mathbf{\Delta} \equiv \mathbf{H}\mathbf{\Delta}, \tag{30}$$

$$\boldsymbol{\sigma} = \mathbf{C}\mathbf{H}\mathbf{\Delta}, \tag{31}$$

where **D** and **C** are defined above and the **H** matrix is constructed as

$$\mathbf{H} = \begin{bmatrix} \frac{\partial \mathcal{R}_0^{p,q}}{\partial x} & 0 & \frac{\partial \mathcal{R}_1^{p,q}}{\partial x} & 0 & \dots & \frac{\partial \mathcal{R}^{p,q}_{(n_1+1)(n_2+1)-1}}{\partial x} & 0 \\ 0 & \frac{\partial \mathcal{R}_0^{p,q}}{\partial y} & 0 & \frac{\partial \mathcal{R}_1^{p,q}}{\partial y} & \dots & 0 & \frac{\partial \mathcal{R}^{p,q}_{(n_1+1)(n_2+1)-1}}{\partial y} \\ \frac{\partial \mathcal{R}_0^{p,q}}{\partial y} & \frac{\partial \mathcal{R}_0^{p,q}}{\partial x} & \frac{\partial \mathcal{R}_1^{p,q}}{\partial y} & \frac{\partial \mathcal{R}_1^{p,q}}{\partial x} & \dots & \frac{\partial \mathcal{R}^{p,q}_{(n_1+1)(n_2+1)-1}}{\partial y} & \frac{\partial \mathcal{R}^{p,q}_{(n_1+1)(n_2+1)-1}}{\partial x} \end{bmatrix}. \tag{32}$$

It should be noted that in the FGM analysis, the components of the constitutive matrix, in general, are functions of the coordinates of the points. In order to evaluate the integral expression of stiffness matrix, it is necessary to express these functions in terms of NURBS parameters. As mentioned before, similar to the FE method, two different concepts exist for this purpose. First, direct sampling of the material properties variations, in which it suffices to substitute the coordinates X and Y in terms of parametric coordinates, i.e.

$$X(r,s) = \sum_{i=0}^{n}\sum_{j=0}^{m} \mathcal{R}_{ij}^{p,q}(r,s) X_{i,j}, \tag{33}$$

$$Y(r,s) = \sum_{n}^{i=0}\sum_{m}^{j=0} \mathcal{R}_{ij}^{p,q}(r,s) Y_{i,j}, \tag{34}$$

into the function assumed for variations of material properties. Second, employing the generalized isoparametric formulation, in which the variations of material properties are approximated by using the NURBS basis functions in a similar fashion to the displacement components as

$$E(r,s) = \sum_{n_1}^{i=0}\sum_{n_2}^{j=0} \mathcal{R}_{ij}^{p,q}(r,s) E_{ij}, \tag{35}$$

in which E_{ij} denotes the altitudes of control points that generate an imaginary surface where the height of the surface at any point correspond to the value of the elastic modulus.

For the isotropic functionally graded materials, only the modulus of elasticity is assumed to vary throughout the domain of interest and consequently can be stated in terms of NURBS parameters by using Eq. (34). Likewise, for the orthotropic FGMs, which are also considered in this research, the similar relation as (34) should be written for three independent material properties; i.e. E_{11}, E_{22}, G_{12}.

On the other hand, in the generalized isoparametric concept, we are intended to use the same net of control points for interpolation of material properties variations throughout the domain as well as the geometry and the analysis. Therefore, the mentioned algorithms in Section 2.4, are not of interest in this concept and cannot be utilized except in some special cases. Because, in the mentioned interpolation techniques, all the coordinates of control points are unknowns which are produced by the algorithm, whereas we have already prescribed some coordinates of the control points as well as the knot vectors for the definition of the geometry.

Thus, we must employ an algorithm wherein the only unknowns to be determined are the altitudes of control points in a manner that the obtained imaginary surface interpolates the material properties variations as precise as possible. For the sake of better insight, a typical square physical domain with its defining control points is depicted in Fig. 3(a). Fig. 3(b) and (c) demonstrate typical interpolator surfaces of the materials variations and the resulted field variable, respectively. As the figures show, the coordinates x and y of the control points are the same as those of physical domain in all the surfaces. A devised algorithm for this purpose is briefly explained in the following.

Assume a NURBS surface as Eq. (3) is the surface which interpolates the variations of the desired material property as is typically shown in Fig. 3(b). Similar to the most of other interpolation techniques, we assume all the weighting coefficients equal to unity. So, we obtain a B-Spline surface which can be written as

$$\mathbf{S}(u,v)=\sum_{i=0}^{n}\sum_{j=0}^{m}N_{i,p}(u)N_{j,q}(v)\mathbf{P}_{i,j}, \tag{36}$$

where $\mathbf{P}_{i,j}$ is the net of control points that includes the following coordinates

$$\mathbf{P}_{i,j}=\begin{Bmatrix}X_{i,j}\\ Y_{i,j}\\ Z_{i,j}\end{Bmatrix}. \tag{37}$$

According to previous explanations, the algorithm is supposed to approximate the variations of a desired function, wherein the coordinates $X_{i,j}$, $Y_{i,j}$ are prescribed, as well as the knot vectors **U** and **V**, and the only unknowns to be determined are the coordinates $Z_{i,j}$. Substituting Eq. (36) into (35) yields an extra relation to Eqs. (32) and (33) for the third coordinate as

$$Z(r,s)=\sum_{i=0}^{n}\sum_{j=0}^{m}N_{i,p}(r)N_{j,q}(s)Z_{i,j}, \tag{38}$$

in which $Z_{i,j}$ are the $(n+1)(m+1)$ unknowns to be determined. Now selecting $(n+1)(m+1)$ arbitrary points in the parametric space and substituting in (32) and (33), yields the corresponding coordinates X and Y in the Cartesian coordinate system. By having the exact values of the desired material property at these coordinates from the assumed analytical function, and substituting into the left side of Eq. (37), a system of linear algebraic equations is constructed which yields the desired unknowns $Z_{i,j}$.

As seen above, employing the generalized isoparametric formulation in the IGA method is not as easy as in the FEM and requires more computations. However, it has some advantages over the isoparametric graded finite elements such as higher continuity of material properties in the entire domain as well as more accuracy and smoother interpolation of material gra-

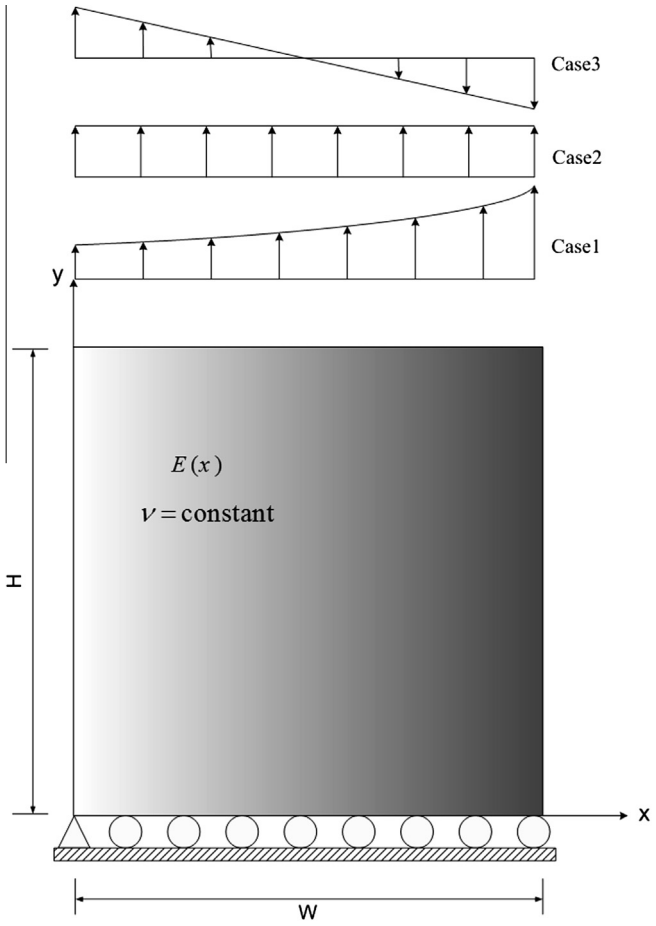

Fig. 4. Square isotropic FG plate subjected to various loadings.

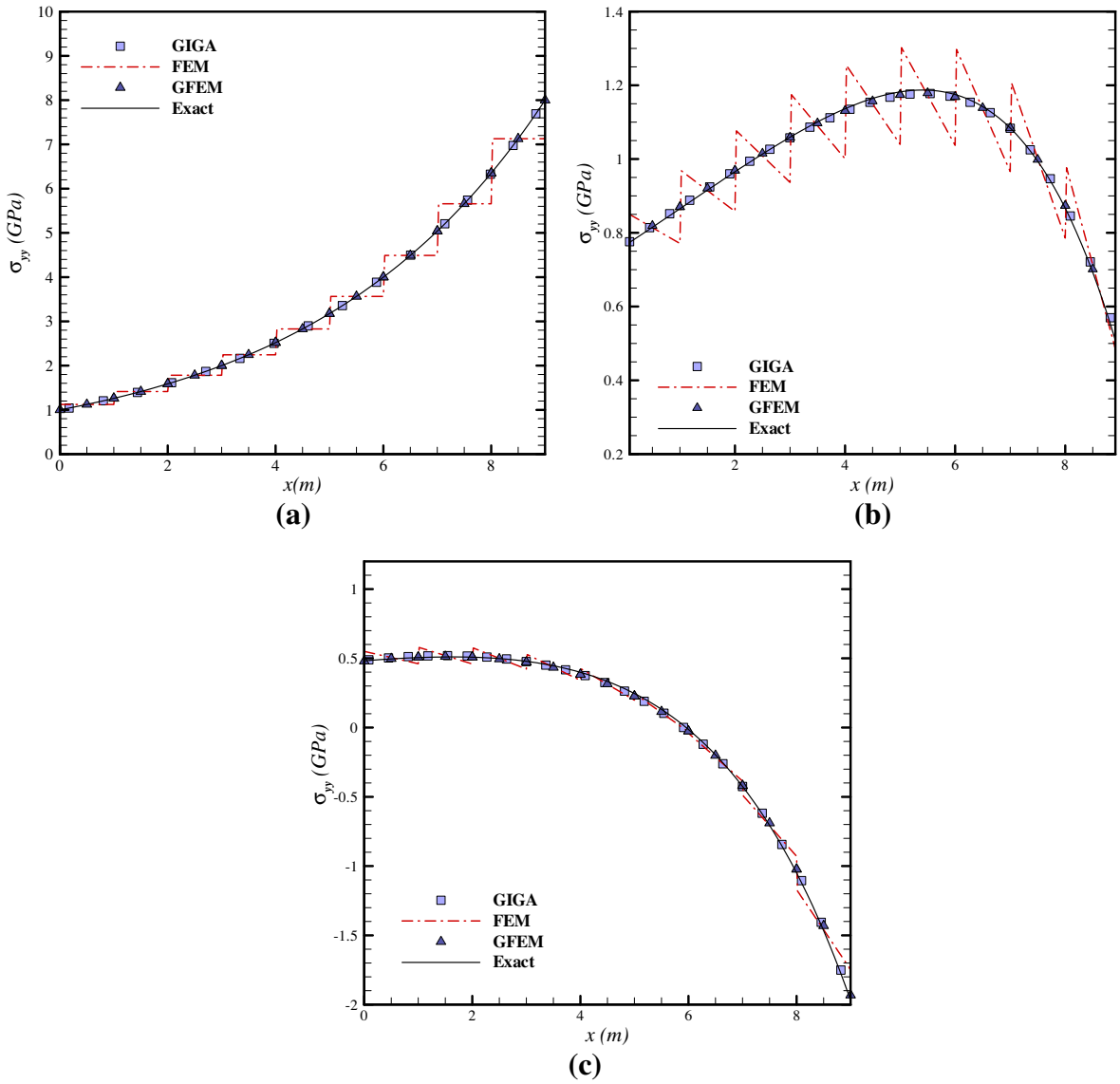

Fig. 5. Distribution of σ_{yy} at $y = 0$ for FG plate subjected to (a) fixed-grip load (b) tensile load (c) bending load.

Table 1
The errors measured in L^2-norm of the vertical stress.

Loading condition	FEM	GFEM	GIGA
Tension	0.0637	0.0161	0.0157
Bending	0.1229	0.0321	0.0315

dations, that is due to the high interpolation abilities of B-Splines and NURBS in comparison with the finite element shape functions.

Although in problems that there are prescribed analytical functions for variations of the material properties we can also employ the direct approach, it is inevitably utilized in problems where there are not definite analytical functions for variations of material properties. A material distribution optimization problem in which we intend to design the appropriate distribution of material constituents of an FGM can be mentioned as a practical example. Furthermore, implementation of the generalized formulation into a computational code is easier and more routine. By employing the generalized formulation, it is just required to prepare some numerical data, i.e. the altitudes of control points corresponding to imaginary surfaces of

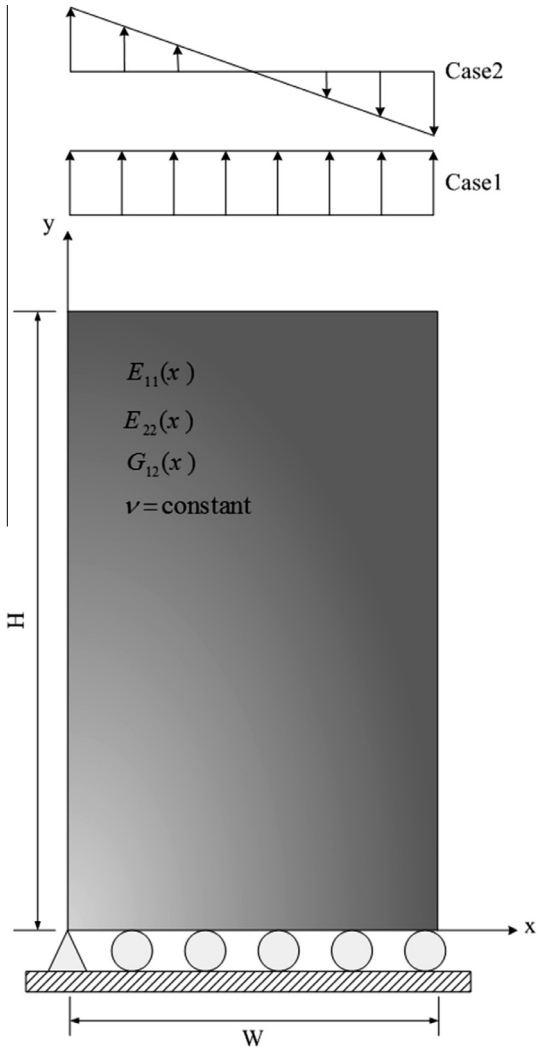

Fig. 6. Rectangular orthotropic FG plate subjected to various loadings.

each desired material property, for the analysis. So, the values of the material properties will be interpolated at the Gauss points by employing the same basis functions used for the definition of the geometry and the analysis.

Now, quite similar to the isoparametric finite elements, and employing all the approximations pointed out formerly, the integrands will be transformed in terms of the knot parameters r and s. Following the mapping of the functions from the Cartesian into the parametric coordinates, for numerical integration the Jacobi matrix is needed where its Jacobean is written as

$$\mathcal{J}(r,s) = \begin{vmatrix} \frac{\partial X(r,s)}{\partial r} & \frac{\partial Y(r,s)}{\partial r} \\ \frac{\partial X(r,s)}{\partial s} & \frac{\partial Y(r,s)}{\partial s} \end{vmatrix}, \tag{39}$$

Following a procedure similar to the FEM with the standard variational method results in a system of linear equations

$$\mathbf{Ku} = \mathbf{f}, \tag{40}$$

where $\mathbf{K}$ is the matrix of coefficients and $\mathbf{f}$ is the force vector. For more explanations reference [1] can be consulted. In order to evaluate the efficiency of the proposed method based on the formulation that was shortly explained above, a computer program in FORTRAN language was developed and employed to solve the examples that follow.

4. Some experiences with the method

To demonstrate the performance and accuracy of the method, four numerical examples are presented. The solutions of the examples are compared with available analytical solutions as well as the results of the conventional and graded FEM.

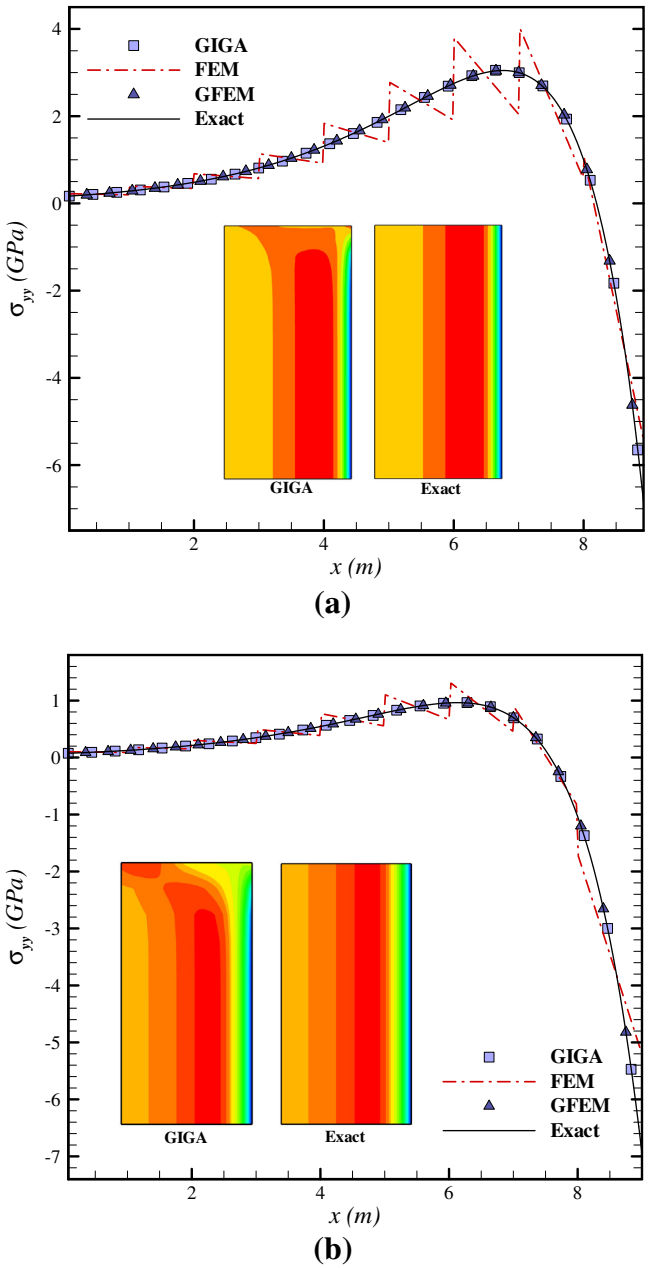

Fig. 7. Distribution of σ_{yy} at $y = 0$ for FG plate subjected to (a) tensile load (b) bending load.

The conventional FEM is referred to the solution method for graded property of a material by treating it as a piece-wise homogeneous material, where the location at the center of each element is used as a reference for material property calculation. It must be mentioned that in all the examples, quadratic basis functions together with uniform knot vectors in both directions have been employed for the analysis using the GIGA approach. Moreover, linear parameterization is employed for modeling of all the examples geometries. Also, for the sake of possibility of comparison, an 8-noded element with quadratic shape functions known as 'serendipity' element has been employed for the analysis by using the FEM. Furthermore, it is assumed that the employed units for different quantities are consistent in all the examples.

All the presented examples are available in the literature, so in order to avoid the redundancy, the interpretation of the results concerning the behavior of FGMs in comparison with corresponding homogeneous cases, which is not the main scope of this research, are discussed briefly in the paper and the interested reader is suggested to refer to the previous published works. In order to gain a better quantitative insight to the computational efficiency of GIGA, the consumed computational time of the proposed method for some of the examples are also presented. It needs to be mentioned that the programs are compiled on a laptop computer with Intel Core2 Duo CPU-2.40 GHz and 2 GB of RAM.

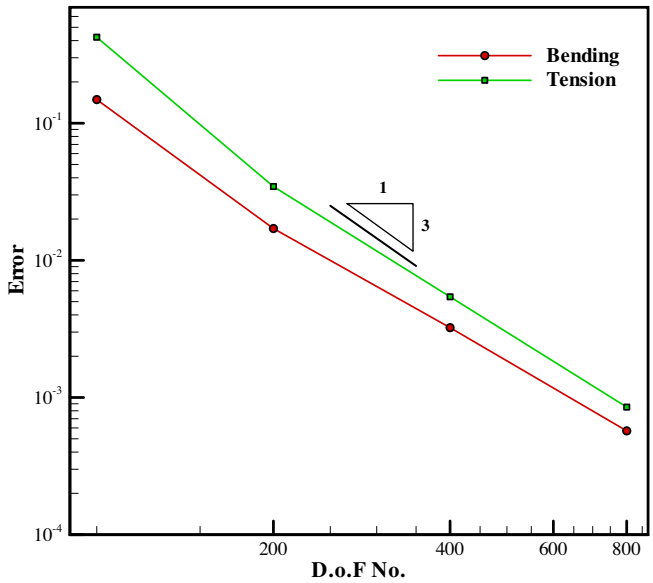

Fig. 8. Errors measured in L^2-norm of the vertical stress for different loading conditions.

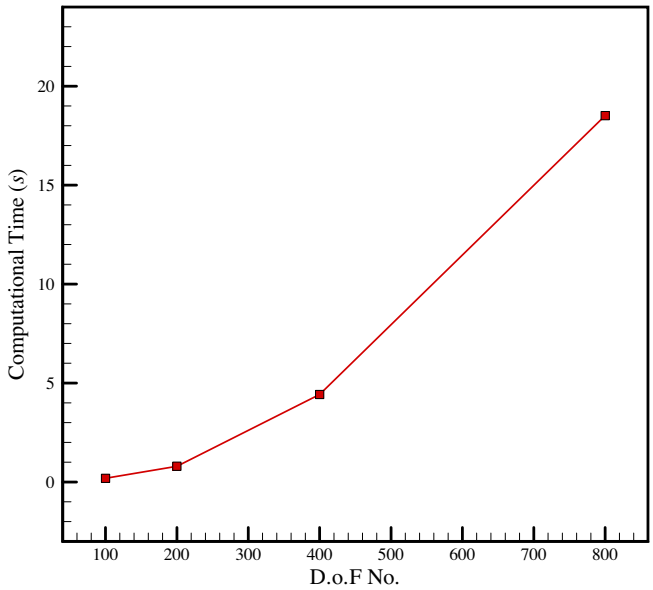

Fig. 9. Computational time of GIGA for the analysis of the FG plate.

4.1. Isotropic FG square plate subjected to various loadings

A square plate with constant thickness made of a nonhomogeneous isotropic material under the generalized plane stress conditions, as shown in Fig. 4, is considered. The Poisson's ratio is constant, $v = 0.3$, and the variation of the Young's modulus is assumed to have the exponential form of Eq. (40), from $E_1 = 1$ GPa at the left edge to $E_2 = 8$ GPa at the right side. The dimensions of the plate are $W = H = 9$ m, and its thickness is equal to unity.

$$E(x) = E^0 \exp(\beta x). \tag{41}$$

The elasticity modulus at the left side of the plate is taken as E^0 and the non-homogeneity parameter β, which dictates the profile of the material gradation with horizontal coordinate is assumed as

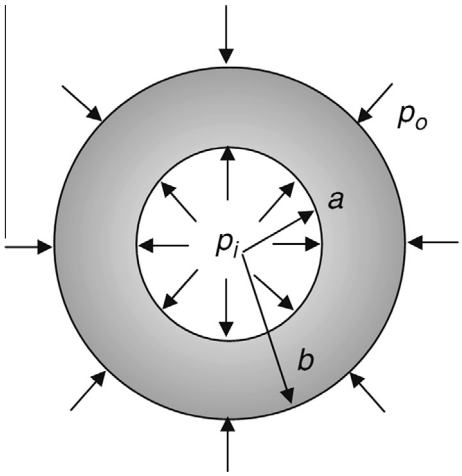

Fig. 10. Hollow cylindrical domain under uniform pressure.

$$\beta = \frac{1}{W}\log\left(\frac{E(W)}{E(0)}\right), \tag{42}$$

where W is the width of the FGM plate as shown in Fig. 4. Note that the parameter β is not dimensionless and has unit $[m^{-1}]$. The analytical solutions for an infinite plate with different boundary conditions can be taken from [13] as follows.

For fixed grip loading with $\varepsilon_{yy}(x, \pm\infty) = \varepsilon_0$ the stress distribution becomes

$$\sigma_{yy}(x) = E^0\varepsilon_0 \exp(\beta x). \tag{43}$$

The corresponding tractions at the end points of the plate are schematically shown in case 1 of Fig. 4. As the second case, a uniform distributed tensile load of intensity $\bar{f}_y = 1$ GPa applied at the top edge of the plate, as is shown in case 2 of Fig. 4, is considered. For this loading case, the analytical solution for the stress distribution is obtained as

$$\sigma_{yy}(x) = E^0 \exp(\beta x)(Ax + B), \tag{44}$$

where the constants A (with dimension $[\text{length}]^{-1}$) and B (dimensionless) are determined by Eqs. (44) and (45) respectively.

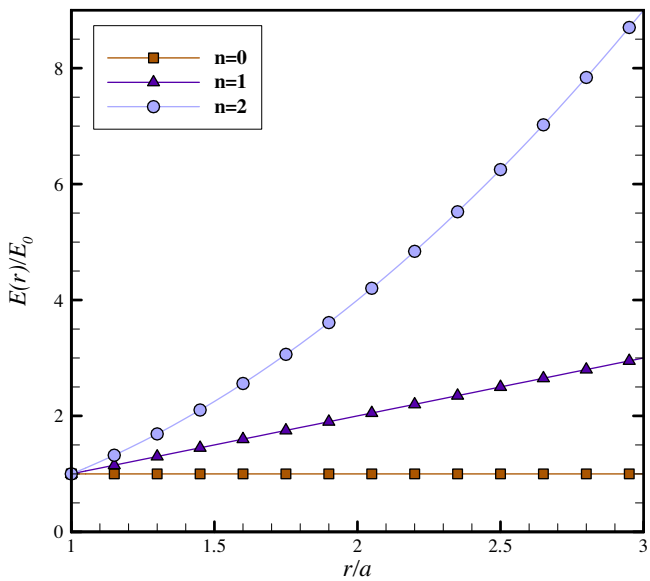

Fig. 11. Gradation in Young's modulus for different values of the power-law exponent.

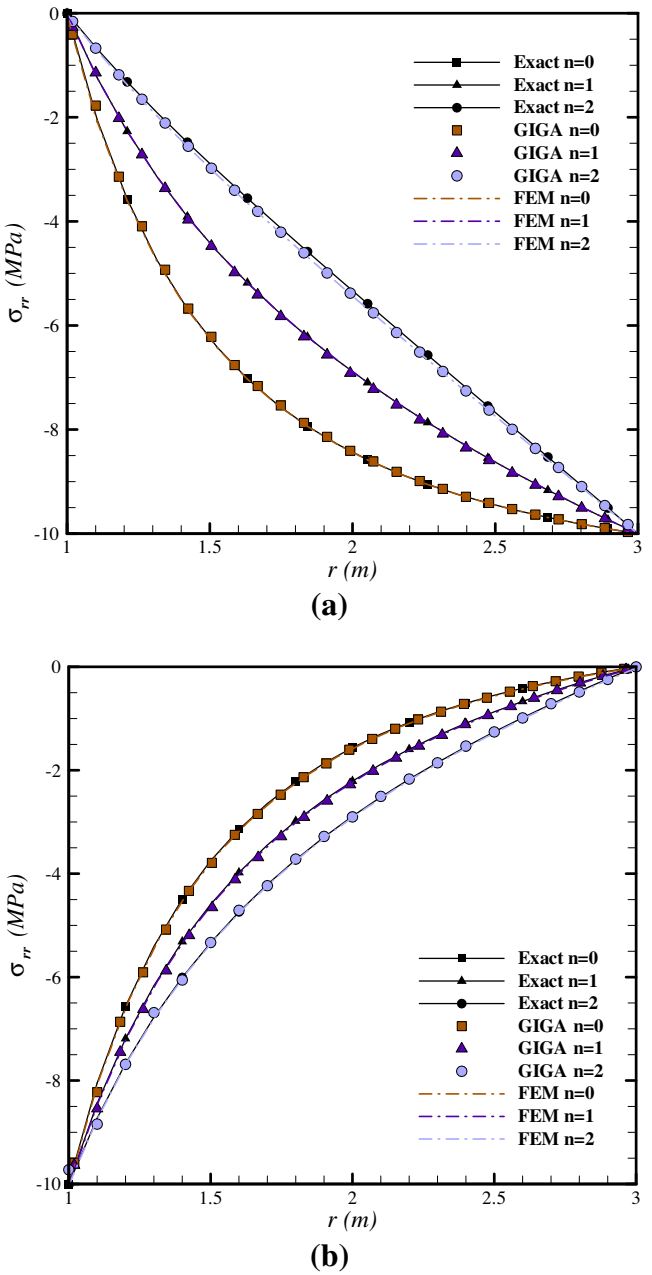

Fig. 12. Radial stress distribution in hollow FG cylinder under (a) internal pressure (b) external pressure.

$$A = \frac{\beta N}{2E^0}\left(\frac{W\beta^2 e^{\beta W} - 2\beta e^{\beta W} + W\beta^2 + 2\beta}{e^{\beta W}\beta^2 W^2 - e^{2\beta W} + 2e^{\beta W} - 1}\right), \tag{45}$$

and

$$B = \frac{\beta N}{2E^0}\left(\frac{e^{\beta W}\left(e^{\beta W}(-W^2\beta^2 + 3\beta W - 4) + \beta^2 W^2 - 2\beta W + 8\right) - \beta W - 4}{(e^{\beta W} - 1)\left(e^{\beta W}\beta^2 W^2 - e^{2\beta W} + 2e^{\beta W} - 1\right)}\right). \tag{46}$$

In the last case, a bending load according to Eq. (46), which is applied to the top edge of the plate, as shown in case 3 of Fig. 4, is considered.

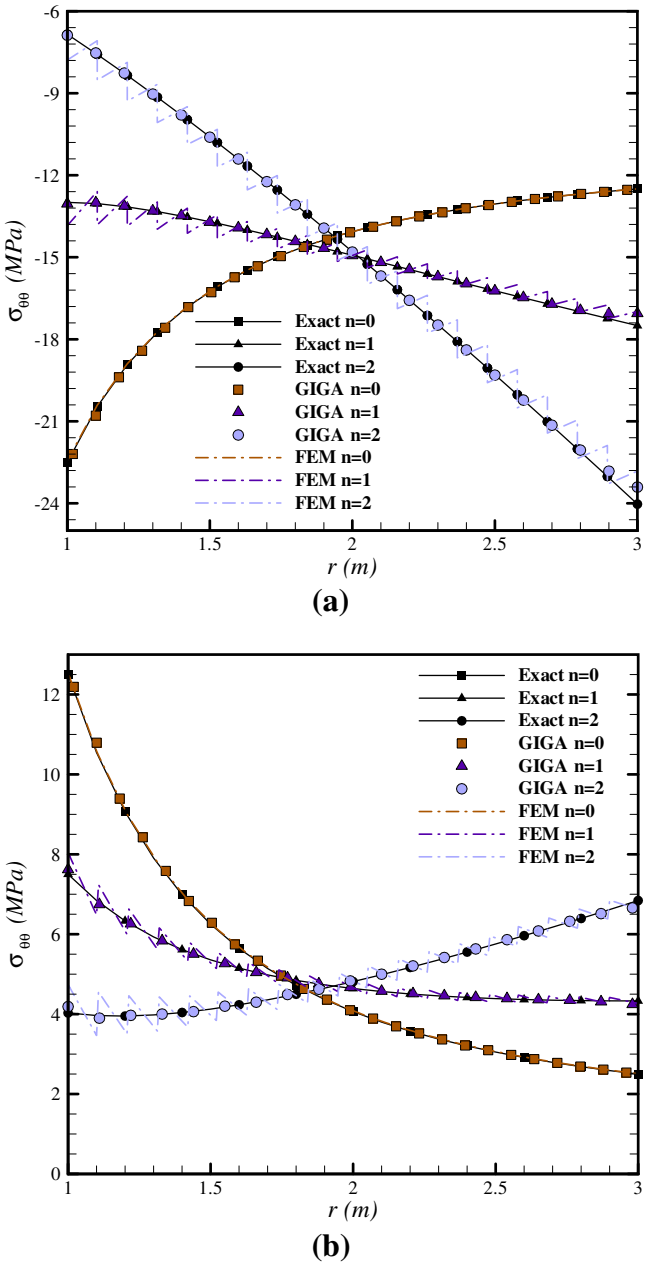

Fig. 13. Hoop stress distribution in hollow FG cylinder under (a) internal pressure (b) external pressure.

$$\bar{f}_y = \left[1 - \frac{2}{9}x\right] \text{GPa}. \tag{47}$$

The closed form solution of the stress distribution for this loading case is again given by Eq. (43), where the coefficients A and B are determined using the following equations

$$A = \frac{\beta^2 M}{E^0}\left(\frac{\beta(1-e^{\beta W})}{e^{\beta W}\beta^2 W^2 - e^{2\beta W} + 2e^{\beta W} - 1}\right), \tag{48}$$

$$B = \frac{\beta^2 M}{E^0}\left(\frac{\left(\beta W e^{\beta W} - e^{\beta W} + 1\right)}{e^{\beta W}\beta^2 W^2 - e^{2\beta W} + 2e^{\beta W} - 1}\right). \tag{49}$$

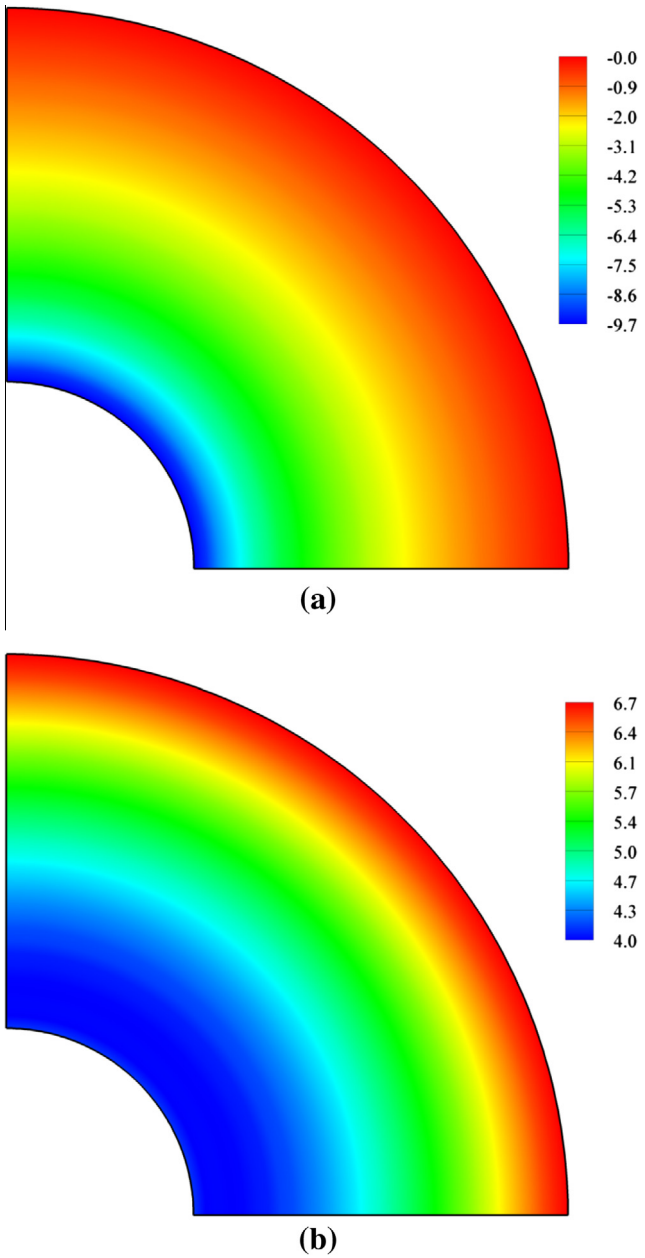

Fig. 14. The contours of the (a) radial, and (b) hoop stress components, for the special case of under internal pressure with $n = 2$.

Table 2
The errors measured in L^2-norm of the radial and hoop stresses.

Stress component	Power law exponent	FEM	GFEM	GIGA
σ_{rr}	$n = 0$	0.1731	0.1791	0.0806
	$n = 1$	0.1040	0.2547	0.1121
	$n = 2$	0.0880	0.3737	0.1636
$\sigma_{\theta\theta}$	$n = 0$	0.1732	0.0455	0.0303
	$n = 1$	0.5778	0.0641	0.0391
	$n = 2$	0.8834	0.0933	0.0579

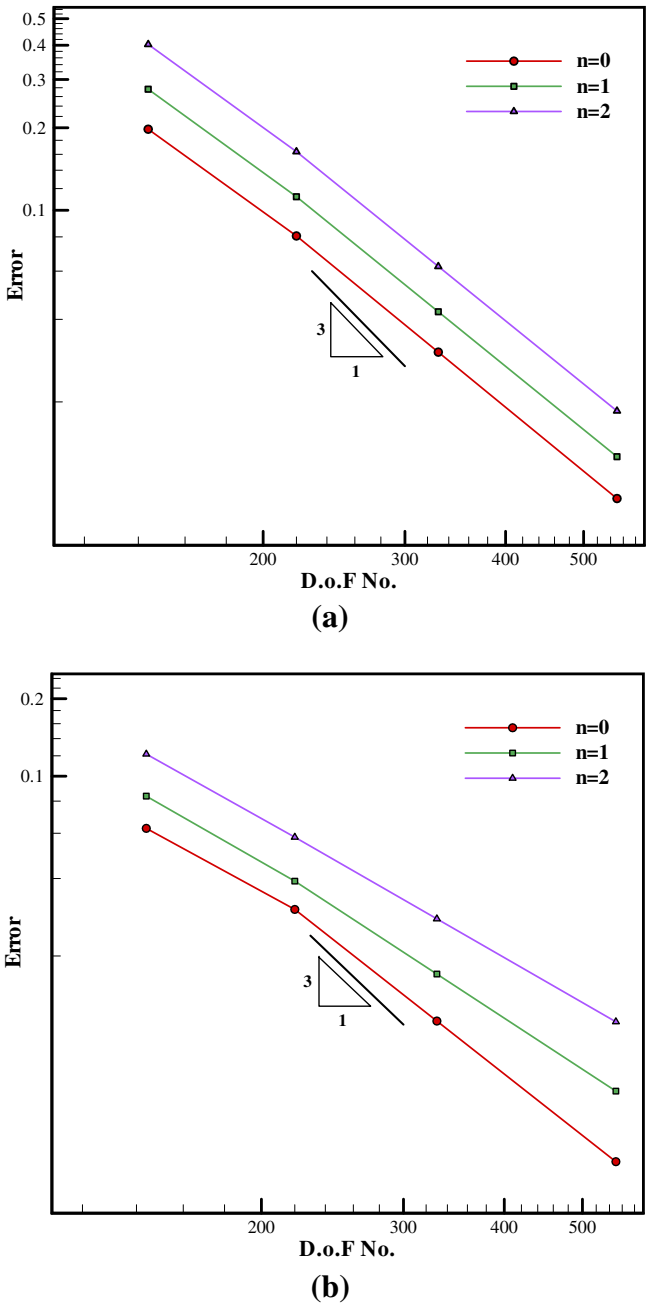

Fig. 15. Errors measured in L^2-norm of the (a) radial (b) hoop stress component, for the special case of under internal pressure.

Now, for the sake of comparison, the problem is solved by using the GIGA method for all loading cases with 100 control points. The obtained results of the presented method together with the exact solutions, as well as the results of the conventional and graded FEM are illustrated in Fig. 5(a)–(c) for the vertical normal stress distribution σ_{yy}. In these figures, the reported results of the conventional and graded FEM are obtained by using a 9×9 mesh of Q8 homogeneous and graded elements, respectively.

In this problem, the vertical stress distribution for the first two loading cases is uniform along the width of the plate for homogeneous material; while, as Fig. 5(a) and (b) show, the stress distribution for graded materials is totally different. As seen in these figures, the maximum vertical stress occurs inside the plate, while the minimum happens at the right end.

In the last loading condition, i.e. pure bending, for the homogeneous material, the obtained distribution for σ_{yy} is linear with zero value at the middle of the plate and the maximum absolute value at the ends; while, as seen in Fig. 5(c), the maximum vertical stress of the left side as well as the position of the zero-value stress shifts to the right.

As the figures demonstrate, the results of the conventional FEM follow a zigzag pattern. This is due to the fact that, as mentioned before, in this approach in order to capture the material gradations, different material properties are assigned to adjacent elements. As a result, the stress evaluated at the common side of these elements differs between the elements. It is noted that in commercial FEM software, in order to avoid this problem, a nodal averaging scheme is adopted for the calculation of the gradient terms which results in continuous predictions for the stress and strain components with a good accuracy except for the regions near the edges.

For the evaluation of the performance of GIGA in comparison with the conventional and graded FEM, the errors in L^2-norm of the vertical stress are obtained for the last two loading cases and reported in Table 1. It is noted that for acquiring the mentioned norm of the error of the conventional FEM, the nodal averaging scheme is employed.

Table 1 shows that, despite employing much fewer degrees of freedom, GIGA yields better accuracy than the conventional and graded FEM. It is noted that the results of GIGA are obtained by employing only 200 degrees of freedoms, while both the conventional and graded FEM result in a system of 560 equations.

4.2. Orthotropic functionally graded rectangular plate

In order to demonstrate the performance of GIGA for orthotropic FGMs, as the second example, an orthotropic functional graded rectangular plate of length $H = 18$ m and width $W = 9$ m, subjected to various loading conditions is considered. The plate is assumed under the generalized plane stress condition. Fig. 6 shows the basic geometry, boundary conditions and material variations of the plate. It is assumed that the two principal Young's moduli (E_{11}, E_{22}) and in-plane shear modulus (G_{12}) vary proportionally with the same exponential function of Eq. (50), wherein the parameters E and β must be replaced with the appropriate material properties, e.g. E_{11}, β_{11} and etc. For instance, for the first principal Young's moduli, it becomes

$$E_{11}(x) = E_{11}^0 \exp(\beta_{11} x), \tag{50}$$

in which

$$\beta_{11} = \frac{1}{W} \log\left(\frac{E_{11}(W)}{E_{11}(0)}\right). \tag{51}$$

Similar relations can be written for E_{22} and G_{12}. In both of the loading cases, the following numerical data were used for the analysis: $E_{11}^0 = 1$ GPa, $E_{22}^0 = 0.1$ GPa, $G_{12}^0 = 0.5$ GPa, $\nu_{12} = 0.3$, $\beta = \log(8)/9$, $\beta_{11} = \beta$, $\beta_{22} = 3\beta$ and $\beta_{12} = 2\beta$. The analytical solutions for the stress distribution of the plate with different loadings can again be obtained by Eqs. (43)–(48), wherein the parameters E^0, β are replaced by E_{22}^0, β_{22} for the present orthotropic case [13].

Numerical results of GIGA, together with the exact solution as well as the results of the conventional and graded FEM, for the vertical stress component, σ_{yy}, are depicted in Fig. 7(a) and (b) for tensile and bending load conditions, respectively. It is noted that in this example the results of GIGA are acquired with a net of 10×19 control points, while a 9×18 mesh of elements is employed for the conventional and graded FEM. All of the observations made for the stress distribution of the previous isotropic example, also hold for the present orthotropic one. In order to gain a better insight to the distribution of the

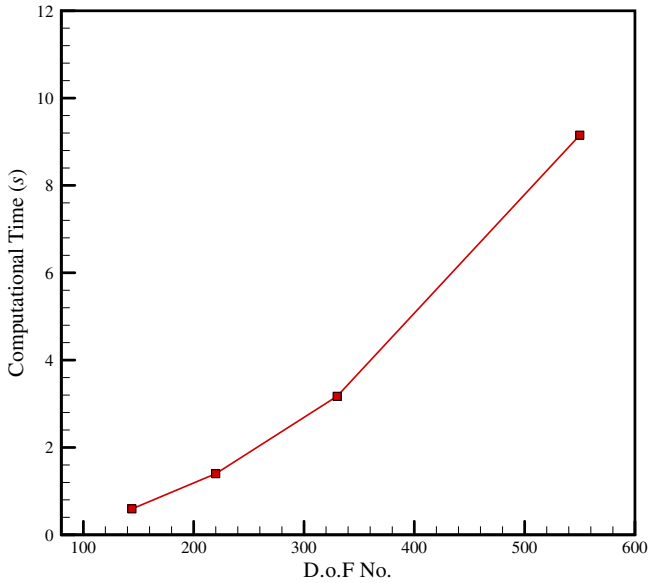

Fig. 16. Computational time of GIGA for the analysis of the FG cylinder.

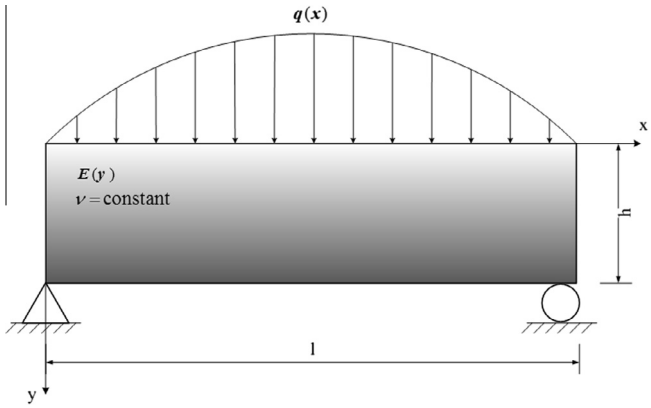

Fig. 17. Geometry and boundary conditions of the FG beam.

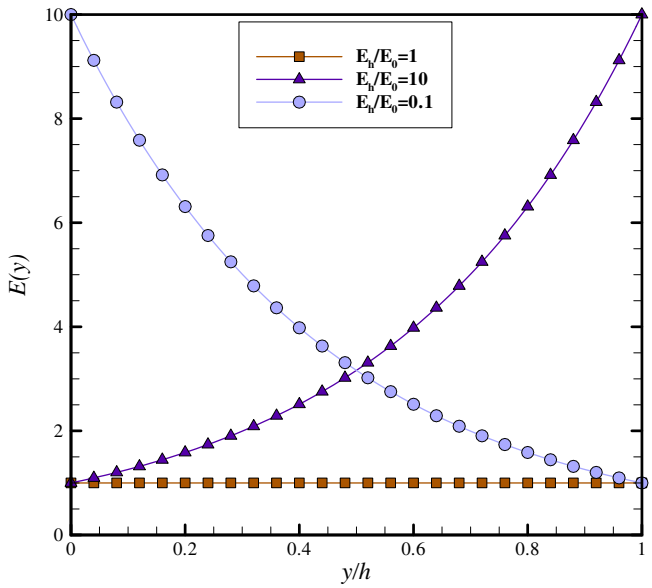

Fig. 18. Gradation in Young's modulus for different values of λ.

stress field throughout the whole structure, the stress contours are also included in the figures. As seen, the figures show good agreements in stress contours of the current and the exact method in most regions of the domain. The little discrepancy observed at the top of the plate, near the loaded boundary, is completely natural and due to the fact that the exact solution is indeed obtained for an infinite plate.

The convergence rate of GIGA is also investigated for this example. To do this, the results of GIGA are acquired for different employed numbers of degrees of freedom by using the h-refinement and employing the linear parameterization; then, the errors are calculated in terms of the L^2-norm of the vertical stress and illustrated in Fig. 8 for both of the loading conditions. As the figure illustrates, in this example, the L^2-convergence rate of stress for the employed quadratic basis functions is approximately three, which is considered as a high rate of convergence.

Furthermore, the consumed computational times for the analysis of this example is also presented in Fig. 9 for different employed numbers of d.o.fs. As the figure clearly shows, the presented computational times, as was expected and similar to the most of other numerical methods, do not follow a linear pattern and increase with a greater slope for higher numbers of d.o.fs.

4.3. A pressurized FG hollow cylinder

In this example, a plane axisymmetric problem of a hollow cylindrical domain under uniform internal and external pressure, as shown in Fig. 10, is considered. The cylinder is assumed to be in the plane stress condition and made up of isotropic

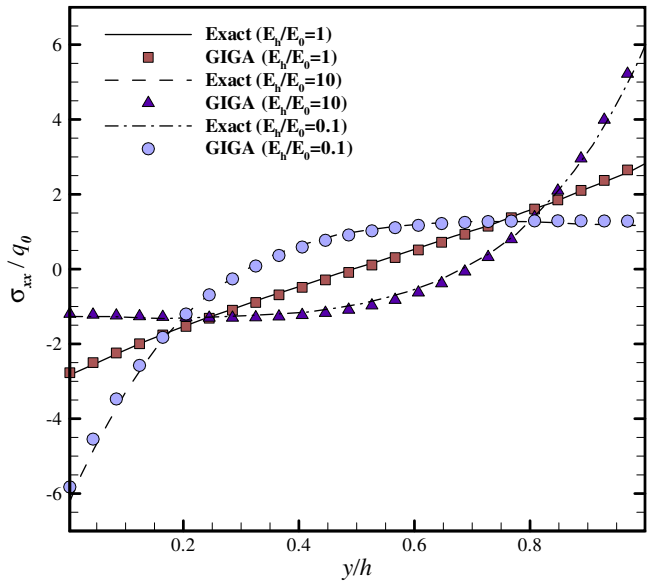

Fig. 19. Distribution of axial stress through the thickness at $x = l/4$.

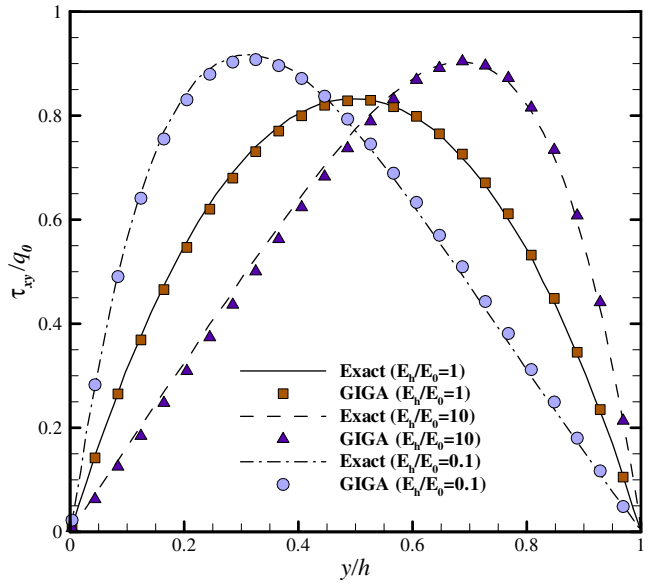

Fig. 20. Distribution of shear stress through the thickness at $x = l/4$.

functionally graded materials. The modulus of elasticity is allowed to be a function of the radial coordinate; that is $E(r)$, and the Poisson's ratio is held constant. Following the work of Horgan and Chan [49], the specific power-law variation for Young's modulus, is considered as

$$E(r) = E_0\left(\frac{r}{a}\right)^n, \tag{52}$$

where E_0 is the value of the elasticity modulus at the inner side of the cylinder, a is the radius of inner boundary of the cylinder and n is the power law exponent. The exact solution for stress distribution of the problem in special cases of only external or internal pressure loading are in the following forms

$$\sigma_{rr} = \frac{p_i a^{(2+k-n)/2}}{b^k - a^k}\left[r^{(-2+k+n)/2} - b^k r^{(-2-k+n)/2}\right], \tag{53}$$

$$\sigma_{\theta\theta} = \frac{p_i a^{(2+k-n)/2}}{b^k - a^k}\left[\frac{2+kv-nv}{k-n+2v} r^{\frac{-2+k+n}{2}} + \frac{2-kv-nv}{k+n-2v} b^k r^{(-2-k+n)/2}\right], \tag{54}$$

for the internal pressure case ($P_o = 0$), and

$$\sigma_{rr} = -\frac{p_0 b^{(2+k-n)/2}}{b^k - a^k}\left[r^{(-2+k+n)/2} - a^k r^{(-2-k+n)/2}\right], \tag{55}$$

$$\sigma_{\theta\theta} = -\frac{p_0 b^{(2+k-n)/2}}{b^k - a^k}\left[\frac{2+k\upsilon-n\upsilon}{k-n+2\upsilon} r^{(-2+k+n)/2} - \frac{2-k\upsilon-n\upsilon}{k+n-2\upsilon} a^k r^{(-2-k+n)/2}\right], \tag{56}$$

for the external pressure case ($P_i = 0$).where $\sigma_{rr}, \sigma_{\theta\theta}$ denote radial and hoop stresses, respectively, and parameter k is obtained from the following equation

$$k = \sqrt{n^2 + 4 - 4nv}. \tag{57}$$

The problem is solved assuming the following numerical values: $a = 1.0$ m, $b = 3.0$ m, $E_0 = 100$ KPa, $v = 0.25$, P_O or $P_i = 10$ MPa. The cylinder is assumed to have a unit length. Due to symmetry, only a quarter of the cylinder is modeled and analyzed. The effect of different material profiles using various values of the power-law exponent in Eq. (530 is also investigated. In order to gain insight into the relative magnitude of such a gradation, Eq. (52) is plotted in Fig. 11 for different values of n. Note that zero value of n indicates a homogeneous material distribution.

The results of GIGA are obtained by using 10 control points in radial direction, while 19 elements in this direction are employed for the FEM analysis. The results for different loadings and material distributions are depicted in Figs. 12 and 13. Fig. 12(a) and (b) demonstrate the distribution of the radial stress σ_{rr}, with respect to radial direction for various degrees of material gradations for the internal and external pressure cases, respectively. It can be seen that the greater values of n dictates less nonlinearity in the profile of the radial stress. As the figure shows, at a fixed r, the magnitude of radial stress increases by increasing the value of n in the internal pressure case, while it decreases under external pressure.

Furthermore, as seen in Fig. 12(a), no discontinuity is observed for the radial stress distribution in conventional FEM results. Likewise, the same observation is expected in all the problems that loadings are applied parallel to material gradation direction and the component of the stress in that direction is under investigation.

On the other hand, the distribution of the hoop stress $\sigma_{\theta\theta}$, with respect to the radial coordinate is illustrated in Fig. 13(a) and (b). The figures show that, in both loading cases, by increasing the value of n, the magnitude of the hoop stress on the internal side of the cylinder up to a specific distance, roughly half thickness, increases and afterwards it is the other way round. It can be seen that for the value of $n = 1$, a nearly uniform distribution of the hoop stress is obtained which is desirable in most of applications. It is also observed that the agreements between GIGA and exact solution gets worse by increasing the value of n, which originates from the relatively small number of control points employed in the radial direction and consequently low-precision approximation of high material gradation and more complicated stress behavior. Accordingly, in order to obtain more accurate results by employing the proposed method for the analysis of problems with high material gradations, more number of control points in the direction of the gradation or a better parameterization is required.

The contours of radial and hoop stress components are also depicted in Fig. 14(a) and (b) for the special case of internal pressure loading with $n = 2$. Comparison of these two figures reveals that the depicted stress components follow opposite patterns. The maximum absolute value of the radial stress component happens at the inner side of the cylinder and has a high gradation near this side, while the maximum absolute value of the hoop stress occurs on the outer side of the cylinder with a high gradation at its vicinity. Furthermore, it is observed that, due to axisymmetry, the stress components do not vary in the hoop direction.

In order to compare the accuracy of different methods, the errors of different methods are calculated in terms of the L^2-norm of the stress components by employing nearly similar degrees of freedom and presented in Table 2. It is noted that the presented results of GIGA are obtained by employing a net of 10×15 control points (300 d.o.f), while the results of the conventional and graded FEM are obtained by using a 5×8 mesh of elements (294 d.o.f). Moreover, it should be mentioned that the presented norms of errors of the conventional FEM are obtained by employing the nodal averaging scheme.

As the table clearly shows, GIGA yields much better accuracy compared to the conventional and graded FEM by using similar numbers of degrees of freedom. It can also be seen that the conventional FEM yields highly accurate results when the stress component under investigation is parallel to the material gradation direction. The same observation is reported in [13].

Furthermore, in this example, the convergence rate of GIGA is also investigated for different employed material profiles in the special case of under internal pressure. The graphs of the errors in terms of the L^2-norm of the radial and hoop stresses are demonstrated in Fig. 15(a) and (b), respectively. Considering the graph, we can observe that both of the stress components follow a nearly similar convergence pattern; however, the results for the hoop stress component have a better accuracy by the same number of degrees of freedom. Moreover, it is observed that the rate of the convergence is not highly dependent on the employed material profile, especially for the radial stress component.

The corresponding computational times for the analysis of the FG cylinder are also demonstrated in Fig. 16. The reported consumed times belong to the special loading case of internal pressure with $n = 2$, which is nearly the same for other mate-

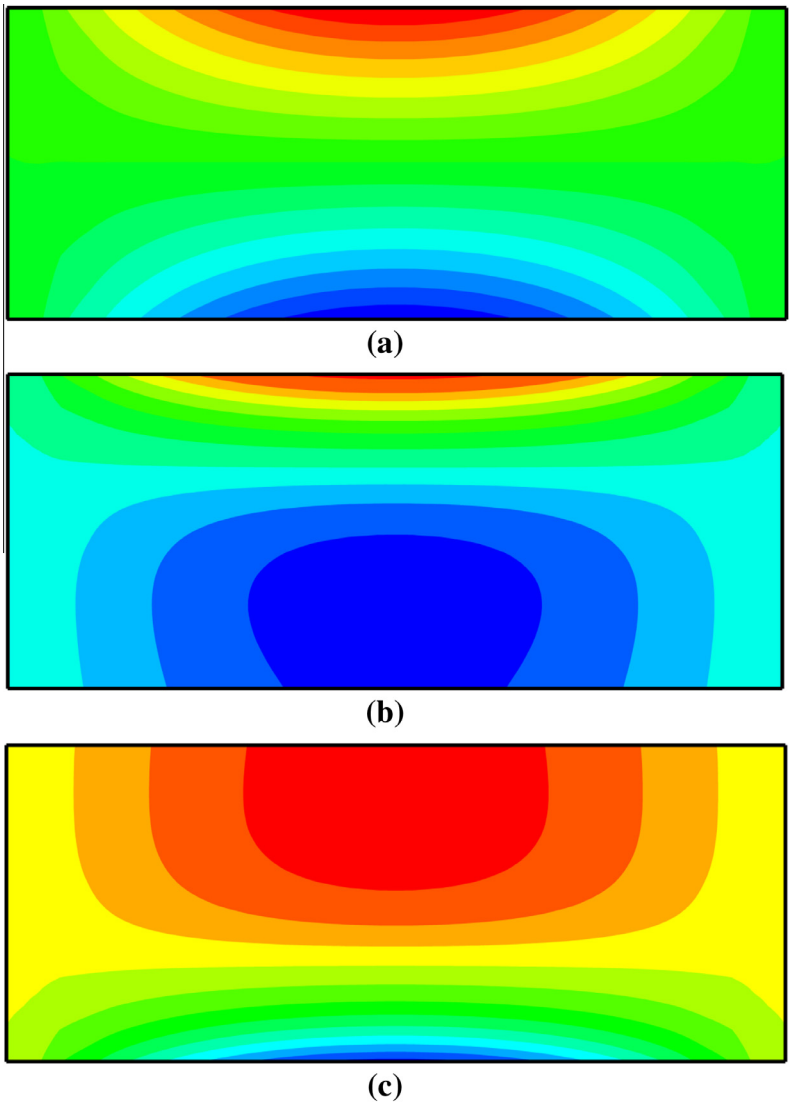

Fig. 21. The axial stress contours for (a) $E_h/E_0 = 1$ (b) $E_h/E_0 = 10$ (c) $E_h/E_0 = 0.1$.

rial profiles and loading conditions. Considering this figure and comparing it to that of the previous example, we can observe that they follow a similar pattern so that in this case the computational effort also rises with a higher rate when more numbers of d.o.fs are employed.

4.4. A simply supported isotropic FG beam

The last example deals with a simply supported isotropic FG beam with material properties varying through the thickness. The beam is subjected to a distributed transverse loading as Eq. (58) on its upper surface. The schematic of the beam with its boundary conditions is shown in Fig. 17. The aspect ratio of the beam is taken to $l/h = 2.5$.

$$q(x) = q_0 \sin(\pi x/l), \tag{58}$$

where q_0 is a constant and l is the length of the beam. Similar to the previous examples, the Poisson's ratio v, is assumed to be constant while the Young's modulus varies exponentially through the thickness of the beam according to the following relation

$$E = E_0 \exp(\lambda y/h), \tag{59}$$

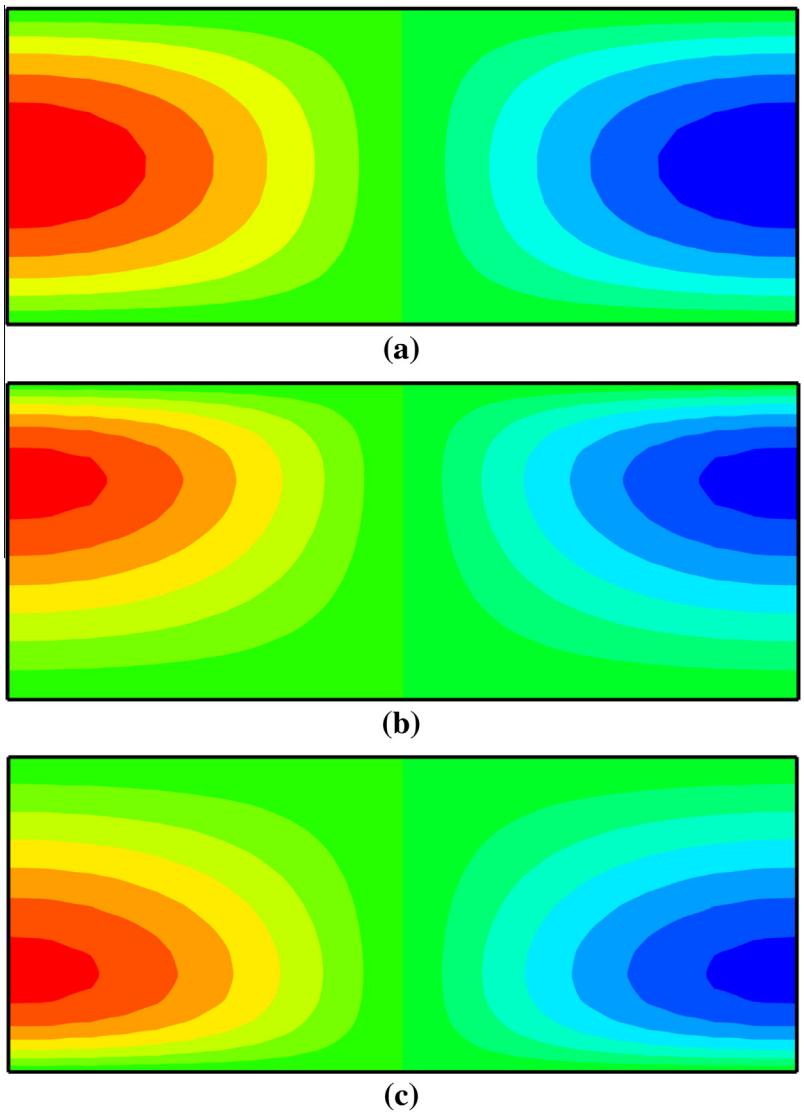

Fig. 22. The shear stress contours for (a) $E_h/E_0 = 1$ (b) $E_h/E_0 = 10$ (c) $E_h/E_0 = 0.1$.

where h is the thickness of the beam, E_0 is the modulus of elasticity at $y = 0$, and λ is a constant that dictates the profile of gradation through the thickness of the beam. The exact elasticity solution of the beam under the plane stress condition is reported by Huang et.al. [50], which is used for validation of our numerical results that follow.

Numerical results are obtained for three different profiles of material gradations including $\lambda = 0$, i.e. the homogeneous case, $\lambda = \log(10)$ and $\lambda = \log(0.1)$. The material profiles for the mentioned values of λ are depicted in Fig. 18 for the sake of better insight. As the figure shows, the selected values for parameter λ, corresponds to the values of 1, 10 and 0.1 for the ratio E_h/E_0. It must be mentioned that the results of GIGA are obtained by using a net of 25×15 control points and uniform knot vectors in both directions.

The distribution of the axial stress component σ_{xx}, with respect to the coordinate y, at $x = l/4$ is depicted in Fig. 19 for different assumed material gradations. As the figure shows, a linear distribution of axial stress with zero value at the midplane of the beam is observed for the homogeneous case. Also, it is seen that the distribution is symmetric with respect to the midplane. Nevertheless, in the second case, i.e. where $E_h/E_0 = 10$, the material of the upper surface is softer than the lower one and consequently bears less magnitude of stress. So, the distribution of the axial stress becomes nonlinear and asymmetric with less magnitude at the upper surface and more at the lower one, in comparison with the homogeneous case. Therefore, the zero stress value shifts to the right and happens at $y/h = 0.68$. The inverse results can be observed for the last case, so that the zero axial stress value shifts to the left and happens at $y/h = 0.32$. Furthermore, the figure shows good agreements between analytical and GIGA results.

On the other hand, Fig. 20 shows the hyperbolic distribution of shear stress τ_{xy}, with respect to y coordinate for the homogeneous case. Also, it is seen that in this case, the distribution is symmetric about the midplane, and the maximum happens at this plane, while in the FGM cases the distributions become asymmetric and the maximum does not happen at the midplane. As the figure shows, in the second case, where the material of the upper surface is softer than the lower one, the maximum shifts to the right and happens at $y = 0.68$, where the axial stress component vanished. Again, the inverse results are observed for the last FGM case. This figure also shows that the results of the GIGA and the analytical ones perfectly match each other.

Also Figs. 19 and 20 indicate that the gradient of the axial and shear stress components increases significantly near the harder surface, which is the consequence of the assumed high gradations of materials near this surface.

For better visualization of the behavior of FGMs through the whole structure, the contours of axial and shear stress components for different values of E_h/E_0 are illustrated in Figs. 21 and 22, respectively. Figs. 21 and 22(a) show symmetric distribution of stress components with respect to the midplane for the homogeneous case, while as Figs. 21 and 22(b) and (c) show, it does not hold for the FGM cases. It is seen that the distribution of the absolute values of stress components are the opposite of each other for two FGM cases which is caused by the assumptions made for the material gradation profiles.

5. Conclusions

Isogeometric stress analysis of plane elasticity problems with FGMs by employing of graded patches, and using a fully isoparametric formulation together with a new perspective of the standard IGA method named "generalized isogeometrical analysis" has been presented in this work. In order to employ the isoparametric formulation for modeling the material variations, a devised interpolation technique by using B-Splines was introduced. Several numerical examples solved which indicate the high efficiency and accuracy of the proposed method for the analysis of FGM problems. The presented examples demonstrated that the performance of the solution by the presented method is better than the conventional and graded FEMs because of removing the discontinuities in stresses and modeling the variations of materials with higher continuity. Also, this method takes the burden of assigning different material properties to each element in the conventional FE analysis. One of the main advantages of this approach, besides its accuracy in defining the boundary conditions and material properties, is the considerable reduction in the resulted system of equations which is cost effective. It must also be mentioned that the proposed solution procedure is not limited to the analysis of FGM problems and also can be applied to other types of differential equations with non-constant coefficients.

Acknowledgments

The support from Grant provided by the Ferdowsi University of Mashhad is gratefully acknowledged.

References

[1] T.J.R. Hughes, J.A. Cottrell, Y. Bazilevs, Isogeometric analysis: CAD, finite elements, NURBS, exact geometry and mesh refinement, Comput. Methods Appl. Mech. Eng. 194 (2005) 4135–4195.
[2] J.A. Cottrell, T.J.R. Hughes, A. Reali, Studies of refinement and continuity in isogeometric structural analysis, Comput. Methods Appl. Mech. Eng. 196 (2007) 4160–4183.
[3] J.A. Cottrell, A. Reali, Y. Bazilevs, T.J.R. Hughes, Isogeometric analysis of structural vibrations, Comput. Methods Appl. Mech. Eng. 195 (2006) 5257–5296.
[4] A. Reali, An isogeometric analysis approach for the study of structural vibrations, J. Earthquake Eng. 10 (2006) 1–30.
[5] R. Schmidt, J. Kiendl, K.U. Bletzinger, R. Wüchner, Realization of an integrated structural design process: analysis-suitable geometric modelling and isogeometric analysis, Comput. Vision Sci. 13 (2010) 315–330.
[6] Y. Bazilevs, V.M. Calo, T.J.R. Hughes, Y. Zhang, Isogeometric fluid–structure interaction: theory, algorithms, and computations, Comput. Mech. 43 (2008) 3–37.
[7] Y. Bazilevs, V.M. Calo, Y. Zhang, T.J.R. Hughes, Isogeometric fluid–structure interaction analysis with applications to arterial blood flow, Comput. Mech. 38 (2006) 310–322.
[8] Y. Bazilevs, J.R. Gohean, T.J.R. Hughes, R.D. Moser, Y. Zhang, Patient-specific isogeometric fluid–structure interaction analysis of thoracic aortic blood flow due to implantation of the Jarvik 2000 left ventricular assist device, Comput. Methods Appl. Mech. Eng. 198 (2006) 3534–3550.
[9] W.L. Zhang, R. Mo, N. Wan, Q. Zhang, Isogeometric analysis of heat transfer in fluids, Appl. Mech. Mater. 105–107 (2012) 2174–2178.
[10] M. Niino, S. Maeda, Recent development status of functionally gradient materials, ISIJ Int. 30 (1990) 699–703.
[11] T.L. Wu, K.K. Shukla, J.H. Huang, Post-buckling analysis of functionally graded rectangular plates, Compos. Struct. 81 (2007) 1–10.
[12] A.J. Markworth, K.S. Ramesh, W.P. Parks, Modeling studies applied to functionally graded materials, J. Mater. Sci. 30 (1995) 2183–2193.
[13] J.-H. Kim, G.H. Paulino, Isoparametric graded finite elements for nonhomogeneous isotropic and orthotropic materials, J. Appl. Mech.-T. ASME 69 (2002) 502–514.
[14] S. Ueda, Thermal shock fracture in a W–Cu divertor plate with a functionally graded nonhomogeneous interface, J. Therm. Stresses 24 (2001) 1021–1041.
[15] L.C. Guo, N. Noda, L. Wu, Thermal fracture model for a functionally graded plate with a crack normal to the surfaces and arbitrary thermomechanical properties, Compos. Sci. Technol. 68 (2008) 1034–1041.
[16] Y. Feng, Z. Jin, Thermal fracture of functionally graded plate with parallel surface cracks, Acta Mech. Solida Sin. 22 (2009) 453–464.
[17] L.C. Guo, N. Noda, An analytical method for thermal stresses of a functionally graded material cylindrical shell under a thermal shock, Acta Mech. 214 (2010) 71–78.
[18] G.G. Sheng, X. Wang, Non-linear response of functionally graded cylindrical shells under mechanical and thermal loads, J. Therm. Stresses 34 (2011) 1105–1118.
[19] M.B. Nazari, M. Shariati, M.R. Eslami, B. Hassani, Meshless analysis of cracked functionally graded material under thermal shock, Mechanika 84 (2010) 20–27.

[20] Z.Y. Huang, C.F. Lu, W.Q. Chen, Benchmark solutions for functionally graded thick plates resting on Winkler–Pasternak elastic foundations, Compos. Struct. 85 (2008) 95–104.
[21] B. Hassani, A direct method to derive the boundary conditions of the homogenization equation for symmetric cells, Commun. Numer. Methods Eng. 12 (1996) 185–196.
[22] B. Hassani, E. Hinton, A review of homogenization and topology optimization I – homogenization theory for media with periodic structure, Comput. Struct. 69 (1998) 707–717.
[23] B. Hassani, E. Hinton, A review of homogenization and topology optimization II – analytical and numerical solution of homogenization equations, Comput. Struct. 69 (1998) 719–738.
[24] B. Hassani, E. Hinton, Homogenization and Structural Topology Optimization – Theory, Practice and Software, Springer, London, 1998.
[25] C. Chinosia, L.D. Croce, Approximation of functionally graded plates with non-conforming finite elements, J. Comput. Appl. Math. 210 (2007) 106–115.
[26] S. Cho, S.H. Ha, Isogeometric shape design optimization: exact geometry and enhanced sensitivity, Struct. Multidiscip. Optim. 38 (2009) 53–70.
[27] M.H. Santare, Use of graded finite elements to model the behavior of nonhomogeneous materials, J. Appl. Mech.-T. ASME 67 (2000) 819–822.
[28] V. Minutolo, E. Ruocco, S. Ciaramella, Isoparametric FEM vs. BEM for elastic functionally graded materials, Comput. Modell. Eng. Sci. 41 (2009) 27–48.
[29] J. Chareonsuk, P. Vessakosol, Numerical solutions for functionally graded solids under thermal and mechanical loads using a high-order control volume finite element method, Appl. Therm. Eng. 31 (2011) 213–227.
[30] V. Sladek, J. Sladek, I. Markechova, An advanced boundary element method for elasticity problems in nonhomogeneous media, Acta Mech. 97 (1993) 71–90.
[31] Q.T. Bui, A. Khosravifard, C. Zhang, M.R. Hematiyan, M.V. Golub, Dynamic analysis of sandwich beams with functionally graded core using a truly meshfree radial point interpolation method, Eng. Struct. 47 (2013) 90–104.
[32] Q.T. Bui, N.M. Nguyen, C. Zhang, An efficient meshfree method for vibration analysis of laminated composite plates, Comput. Mech. 48 (2011) 175–193.
[33] E. Ruocco, V. Minutolo, Two-dimensional stress analysis of multiregion functionally graded materials using a field boundary element model, Compos. Part B 43 (2012) 663–672.
[34] S. Shojaee, N. Valizadeh, E. Izadpanah, Q.T. Bui, T.V. Vu, Free vibration and buckling analysis of laminated composite plates using the NURBS-based isogeometric finite element method, Compos. Struct. 94 (2012) 1677–1693.
[35] N. Valizadeh, S. Natarajan, O.A. Gonzalez-Estrada, T. Rabczuk, T.Q. Bui, S.P.A. Bordas, NURBS-based finite element analysis of functionally graded plates: static bending, vibration, buckling and flutter, Compos. Struct. 99 (2013) 309–326.
[36] X.Y. Kou, S.T. Tan, A systematic approach for integrated computer-aided design and finite element analysis of functionally-graded-material objects, Mater. Des. 28 (2007) 2549–2565.
[37] J. Ying, C.F. Lu, W.Q. Chen, Two-dimensional elasticity solutions for functionally graded beams resting on elastic foundations, Compos. Struct. 84 (2008) 209–219.
[38] J.N. Reddy, Analysis of functionally graded plates, Int. J. Numer. Methods Eng. 47 (2000) 663–684.
[39] J.H. Kim, G.H. Paulino, Mixed-mode fracture of orthotropic functionally graded materials using finite elements and the modified crack closure method, Eng. Fract. Mech. 69 (2002) 1557–1586.
[40] Y. Bazilevs, L. Beirão Da Veiga, J.A. Cottrell, T.J.R. Hughes, G. Sangalli, Isogeometric analysis: approximation, stability and error estimates for h-refined meshes, Math. Models Methods Appl. Sci. 16 (2006) 1031–1090.
[41] M.R. Dörfel, B. Jüttler, B. Simeon, Adaptive isogeometric analysis by local h-refinement with T-Splines, Comput. Methods Appl. Mech. Eng. 199 (2010) 264–275.
[42] B. Hassani, S.M. Tavakkoli, N.Z. Moghaddam, Application of isogeometric analysis in structural shape optimization, Int. J. Scientia Iranica 18 (2011) 846–852.
[43] B. Hassani, N.Z. Moghaddam, Development of a new numerical method for solution of ordinary differential equations by using spline basis functions, Technical Report No. 1015, Shahrood University of Technology, Iran, 2009. (In Farsi).
[44] B. Hassani, M. Khanzadi, S.M. Tavakkoli, N.Z. Moghaddam, Isogeometric shape optimization of three dimensional problems, in: 8th World Congress on Structural and Multidisciplinary Optimization, Lisbon, Portugal, 2009.
[45] B. Hassani, A.H. Taheri, N.Z. Moghaddam, On the application of isogeometric analysis for optimization of natural frequencies of FGM structures, Acta Mech., submitted for publication.
[46] E.V. Shikin, A.I. Plis, Handbook on Spline for the Users, CRC Press, 1995.
[47] L. Piegl, W. Tiller, The NURBS Book, second ed., Springer-Verlag, New York, 1997.
[48] D.F. Rogers, An Introduction to NURBS, Morgan Kaufmann Publishers, 2001.
[49] C.O. Horgan, A.M. Chan, The pressurized hollow cylinder or disk problem for functionally graded isotropic linearly elastic materials, J. Elast. 55 (1999) 43–59.
[50] D. Huang, H. Ding, W. Chen, Analytical solution and semi-analytical solution for anisotropic functionally graded beam subject to arbitrary loading, Sci. China Ser. G 52 (2009) 1244–1256.